Computer Methods in Biomechanics and Biomedical Engineering, Vol. 2, pp. 201–231
Reprints available directly from the publisher
Photocopying permitted by license only

A Dynamic Optimization Solution for Vertical Jumping in Three Dimensions

FRANK C. ANDERSON and MARCUS G. PANDY*

Department of Mechanical Engineering and Department of Kinesiology, University of Texas at Austin, Austin, Texas 78712, U.S.A.

(Received 19 February 1998; In final form 16 December 1998)

A three-dimensional model of the human body is used to simulate a maximal vertical jump. The body is modeled as a 10-segment, 23 degree-of-freedom (dof), mechanical linkage, actuated by 54 muscles. Six generalized coordinates describe the position and orientation of the pelvis relative to the ground; the remaining nine segments branch in an open chain from the pelvis. The head, arms, and torso (HAT) are modeled as a single rigid body. The HAT articulates with the pelvis via a 3 dof ball-and-socket joint. Each hip is modeled as a 3 dof ball-and-socket joint, and each knee is modeled as a 1 dof hinge joint. Each foot is represented by a hindfoot and toes segment. The hindfoot articulates with the shank via a 2 dof universal joint, and the toes articulate with the hindfoot via a 1 dof hinge joint. Interaction of the feet with the ground is modeled using a series of spring-damper units placed under the sole of each foot. The path of each muscle is represented by either a series of straight lines or a combination of straight lines and space curves. Each actuator is modeled as a three-element, Hill-type muscle in series with tendon. A first-order process is assumed to model muscle excitation-contraction dynamics. Dynamic optimization theory is used to calculate the pattern of muscle excitations that produces a maximal vertical jump. Quantitative comparisons between model and experiment indicate that the model reproduces the kinematic, kinetic, and muscle-coordination patterns evident when humans jump to their maximum achievable heights.

Keywords: Jumping, three-dimensional computer modeling, musculoskeletal simulation

INTRODUCTION

The application of dynamic optimization theory to computer simulation of human movement has accelerated in recent years [1–15]. This interest is driven by the ever-increasing performance of computers. Chow and Jacobson [16] were the first to use dynamic optimization to simulate human movement. These researchers solved a dynamic optimization problem for normal gait using a 5 degree-of-freedom (dof), planar model of the whole body, which was actuated by joint torques. Hatze [17] later solved

*Corresponding author.

TABLE I Comparison of mathematical models used to simulate human movement. Studies are listed chronologically. With the exception of Hatze [42]**, all studies solved a dynamic optimization problem. The model in Hatze [42] was used to produce a forward-dynamics simulation of the long jump. Symbols appearing in the table are: 2D, two-dimensional; and 3D, three-dimensional

Study	Dimension	# Segments	# dof	# Muscles
Chow [16]	2D	5	7	0
Hatze [17]	2D	2	3	5
Levine [71]	2D	2	2	0
Hatze [42]**	3D	17	42	46
Zajac [1]	2D	2	2	1
Davy [2]	2D	3	3	9
Khang [3]	2D	3	3	0
Marshall [72]	2D	5	5	0
Yamaguchi [4]	3D	7	8	10
Pandy [5]	2D	4	4	8
Soest [6]	2D	4	4	6
Ziegler [60]	2D	4	4	20
Kautz [11]	2D	7	1	0
Tashman [10]	3D	4	11	0
Fregly [13]	2D	7	3	0
Shelburne [61]	2D	4	6	22
Selbie [14]	2D	4	4	0
Raash [15]	2D	7	3	30
Present Model	3D	10	23	54

a dynamic optimization problem for kicking using a 3 dof, planar model of the leg. This study was significant because it was the first time that a model incorporating muscles had been used to simulate human movement.

To our knowledge, only Yamaguchi and Zajac [4] and Tashman *et al.* [10] have combined three-dimensional modeling with dynamic optimization theory to simulate whole-body movement (see Table I). In their study of normal gait, Yamaguchi and Zajac [4] developed a 7-segment, 8 dof model of the skeleton, which was actuated by 10 muscles. All joints, except one of the hips, were modeled as single dof hinge joints. Relative movements of the pelvis and the upper body were not modeled in this study, and one foot was hinged to the ground. Tashman *et al.* [10] used a much simpler, 4-segment model to simulate paraplegic gait. Relative movements of the pelvis and upper body were included in the model, as was a more detailed representation of the feet. However, to simulate the actuation provided by an orthoses, joint torques rather than muscle forces were used as inputs.

In this paper, a three-dimensional model of the body is combined with dynamic optimization theory to calculate the pattern of muscle excitations needed to produce a maximal vertical jump. Dynamic optimization, which is a forward-dynamics method, is used because it allows a mathematical model of both the system and the motor task to be included in the formulation of the optimization problem. Static optimization, which is an inverse-dynamics method, does not allow the goal of the motor task to be modeled [18–21]. Vertical jumping is studied because this particular task satisfies two important requirements. First, since the goal is to maximize the height reached by the center of mass of the body during the jump, the performance criterion is relatively unambiguous. Second, maximum-height jumping involves the coordinated motion of all the body segments; therefore, once the optimization problem has been solved and the solution validated by comparing the model results with experimental data, the model may be used to simulate other activities which do not have a well-defined performance criterion (e.g., gait).

MUSCULOSKELETAL MODEL OF THE BODY

The skeleton is represented as a 10-segment, 23 dof, mechanical linkage. Each leg is actuated by 24 muscles, and the upper body is actuated by 6 muscles (Figure 1). Six generalized coordinates are used to define the position and orientation of the pelvis (the base segment) relative to an inertial reference frame fixed on the ground. The remaining nine segments branch out in an open chain from the pelvis (Figure 2; Table II). The head, arms, and torso (HAT) are represented as a single rigid body. Because the model is not rigidly attached to the ground, it can be used to simulate a wide range of activities in which the feet make and break contact with the ground; interaction of the feet with the ground is simulated by a series of springs and dampers.

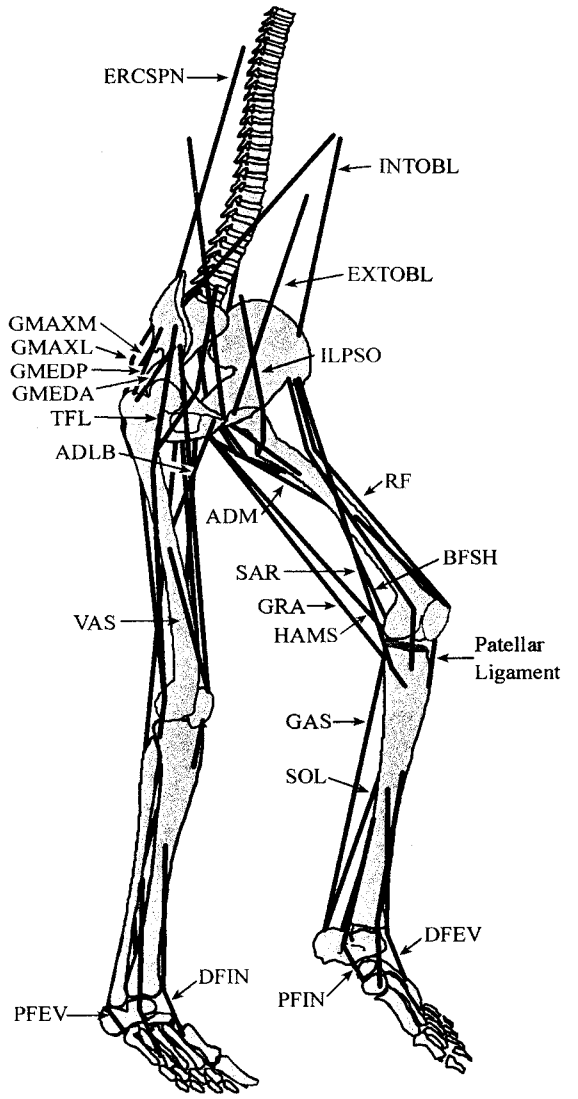

FIGURE 1 Diagram showing the geometry of the 54 muscles in the model. See Table III for abbreviations and parameters. Muscles included in the model but not shown in the diagram are: Piriformis; Pectinius; Flexor Digitorum Longus/Brevis and Flexor Hallucis Longus/Brevis lumped together; and Extensor Digitorum Longus/Brevis and Extensor Hallucis Longus/Brevis lumped together.

Joint Models

The HAT articulates with the pelvis via a 3 dof ball-and-socket joint, which is located approximately at the third lumbar vertebra [10] (Figure 2). A back joint was included in the model in order to separate the motion of the pelvis from that of the more massive HAT segment. Although a single 3 dof back joint is a gross simplification of the kinematic behavior of the human spine, some compromise must be made between reality and model complexity. A more accurate model of the trunk would account for the relative movements of the lumbar and thoracic intervertebral joints [22–25]; however, given the computational resources currently available, a solution to the dynamic optimization problem for jumping would not be possible. The exact location of the back joint in the model was determined by collecting kinematic data as human subjects performed voluntary movements of their pelves and trunks [26].

Each hip is modeled as a 3 dof ball-and-socket joint [27], and each knee is modeled as a 1 dof hinge joint (Figure 2). The direction of the axis of rotation at the knee was determined by collecting kinematic data as subjects flexed and extended their knees [26]. When the model is in its reference configuration, the knee-joint axis of the right leg points 4.6° posteriorly, 2.3° distally, and is assumed to pass through the tibial eminence located between the medial and lateral tibial condyles. Although more detailed models of the knee are available in the

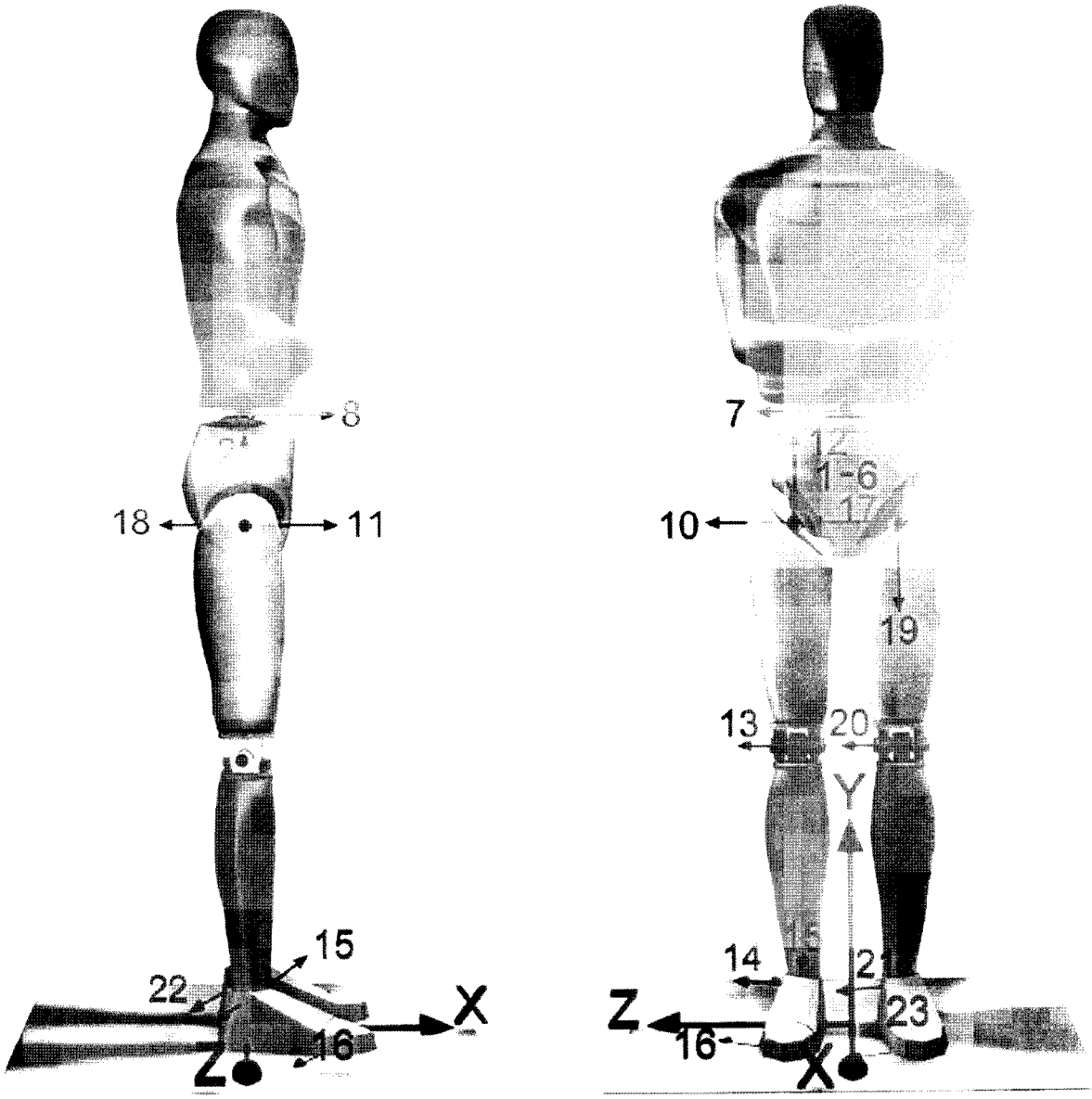

FIGURE 2 Diagram showing the 10-segment, 23 dof model of the skeleton. The numbers indicate the generalized coordinates (q's). The pelvis is the base segment in the model: generalized coordinates q_1-q_3 specify the position of the origin of the pelvis reference frame with respect to the origin of the inertial reference frame fixed on the ground (X,Y,Z); and q_4-q_6 specify the orientation of the pelvis reference frame with respect to the inertial reference frame. On the left side of the body, where appropriate, the axis directions are reversed so that positive changes in the generalized coordinates produce the same anatomical motion. Generalized coordinate q_9 (axial rotation of the HAT) is inside the HAT segment and is not labelled in the figure. See Table II for details.

literature [28–32], a hinge appears to be adequate for simulating multi-joint movement in the lower limb [4,15]. To account for the role of the patella, measured values of the effective moment arm of the quadriceps [33] were used in the model.

Each foot is modeled using two segments: a hindfoot and the toes (Figure 3). The hindfoot articulates with the shank via a 2 dof universal joint, and the toes articulate with the hindfoot via a 1 dof hinge joint. The orientation of the ankle axis was

TABLE II Description of the skeletal model. The structure of the model is specified using the conventions defined in a commercial software package called SD/Fast [53]. The equations of motion can be reproduced using SD/Fast and the numbers below. All parameters are given in the local reference frame of each body with the body in the *reference position*. The *reference position* is the position in which the local reference frame aligns with the inertial reference frame (ground). The local reference frame of each body is located at the center of mass of that body. Each body articulates with an **Inboard Body** by a joint of a particular type. The position of a joint relative to the center of mass of the body is defined by the **Body-To-Joint** vector. The position of the joint relative to the **Inboard Body**'s center of mass is given by the **Inboard-To-Joint** vector. The direction of each joint axis is specified by a normalized vector (**Joint Axes**). The orientation of a body relative to its **Inboard Body** is given by body-fixed Euler angles. The order of rotation is specified by the order of the **Joint Axes**. Mass and the inertia matrix (**I**) are also specified for each body. The model developed in this study has 10 bodies: pelvis, head-arms-torso (HAT), left (l.) and right (r.) thighs, l. and r. shanks, l. and r. hindfeet, and l. and r. toes. The reference position was chosen to be the anatomical position with the arms folded across the torso (see Figure 2). The pelvis is the base segment and articulates with the ground via a 6 dof joint. Each thigh articulates with the pelvis via a 3 dof ball-and-socket joint. Each shank articulates with its thigh via a 1 dof hinge joint. Each hindfoot articulates with its shank via a 2 dof universal joint. Each toes segment articulates with its hindfoot via a 1 dof hinge joint. Mass and **I** for all segments in the model, except the hindfeet and toes, are based on the average anthropometric data obtained for the five subjects. Off-diagonal elements of **I** were neglected to speed computation and because they were small

Body	Inboard Body	Joint Type	Inboard-To-Joint (m)			Body-To-Joint (m)			Joint Axes			Mass (kg)	I ($kg \cdot m^2$)		
pelvis	ground	6 dof		—			—		1	0	0	11.150	0.0973	0.0825	0.0548
									0	1	0				
									0	0	1				
									1	0	0				
									0	1	0				
									0	0	1				
HAT	pelvis	3 dof	0.0000	0.1270	0.0000	0.0000	−0.3202	0.0000	0	0	1	32.413	1.3960	0.7153	1.3552
									1	0	0				
									0	1	0				
r. thigh	pelvis	3 dof	0.0000	−0.0700	0.0935	0.0020	0.1715	0.0000	0	0	1	8.806	0.1268	0.0332	0.1337
									1	0	0				
									0	1	0				
l. thigh	pelvis	3 dof	0.0000	−0.0700	−0.0935	0.0020	0.1715	0.0000	0	0	1	8.806	0.1268	0.0332	0.1337
									−1	0	0				
									0	−1	0				
r. shank	r. thigh	1 dof	0.0033	−0.2294	0.0000	0.0000	0.1862	0.0000	−0.0809	0.0404	0.9959	3.510	0.0477	0.0048	0.0484
l. shank	l. thigh	1 dof	0.0033	−0.2294	0.0000	0.0000	0.1862	0.0000	0.0809	−0.0404	0.9959	3.510	0.0477	0.0048	0.0484
r. hindfoot	r. shank	2 dof	0.0000	−0.2438	0.0000	−0.0359	0.0513	−0.0055	−0.0821	−0.0372	0.9959	1.20	0.0013	0.0037	0.0039
									0.8147	0.5772	−0.0542				
l. hindfoot	l. shank	2 dof	0.0000	−0.2438	0.0000	−0.0359	0.0513	0.0055	0.0821	0.0372	0.9959	1.20	0.0013	0.0037	0.0039
									−0.8147	−0.5772	−0.0542				
r. toes	r. foot	1 dof	0.0980	−0.0380	0.0180	−0.0269	−0.0185	−0.0051	−0.4694	0.0000	0.8829	0.2051	0.0001	0.0002	0.0001
l. toes	l. foot	1 dof	0.0980	−0.0380	−0.0180	−0.0269	−0.0185	0.0051	0.4694	−0.0000	0.8829	0.2051	0.0001	0.0002	0.0001

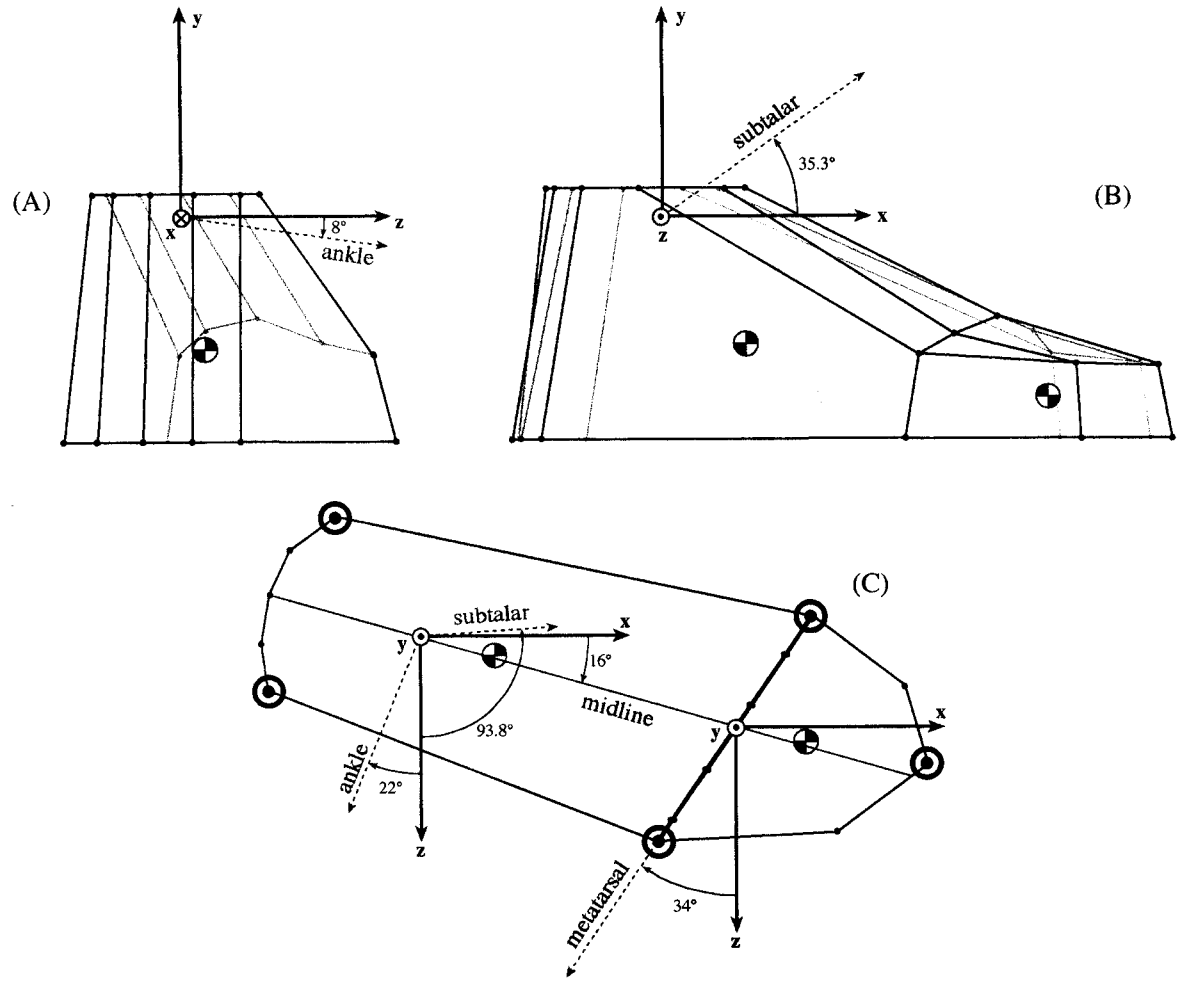

FIGURE 3 Locations of the ankle, subtalar, and metatarsal joint axes for the right foot in the model. The ankle and subtalar axes are projected onto the frontal (A), sagittal (B), and transverse (C) planes. The metatarsal axis is shown in the transverse plane and lies at the sole of the foot (C, metatarsal). The x, y, and z axes define the global reference frame. The vertices and connecting lines represent the volume of a foot plus a size 10 tennis shoe (see text). When the model is in its reference position, the midline of the foot is oriented 16° clockwise from the global x axis (C). Projected onto the transverse plane, the ankle axis is 22° clockwise and the subtalar axis is 93.8° counterclockwise from the global z axis (C). The metatarsal axis is 34° clockwise from the global z axis in the transverse plane (C). Projected onto the frontal plane, the ankle axis is 8° clockwise from the global z axis (A). In the sagittal plane, the subtalar axis is 35.3° counterclockwise from the global x axis (B). The circled dots define the locations of the five ground springs placed under each foot (C).

chosen on the basis of measurements made by Manter [34], Hutter and Scott [35], Barnett and Napier [36], and Isman and Inman [37] and reported by Inman [38]. The orientation of the subtalar axis was determined by collecting kinematic data obtained from human subjects as they plantarflexed, dorsiflexed, inverted, and everted their ankles [26]. The locations of the ankle and subtalar axes were selected using data reported in the literature. Barnett and Napier [36] and Isman and Inman [37] found that the ankle-joint axis passes through two points: one 5 mm distal to the distal tip of the medial malleolus; the other, 3 mm distal and 8 mm anterior to the distal tip of the lateral malleolus. Although a number of studies have shown that the ankle and subtalar axes do not intersect [37–40], for simplicity, we assumed that the joint centers of these axes coincide (Figure 3). Non-intersecting axes would require the

addition of a talus, which, because of its relatively small mass, would increase the integration time for the model considerably.

Model of the Foot-Ground Interface

We considered two options for modeling the interaction between the foot and the ground: 1) using kinematic constraints with Baumgarte stabilization [41]; and 2) using a series of spring-damper units placed under the sole of each foot. Kinematic constraints may be computationally more efficient [42], but they can also be difficult to implement properly, particularly when the constraints come into and out of effect. We chose to model the foot-ground interaction using springs and dampers, but it was first necessary to solve two problems: first, the spring forces must be brought into and out of effect smoothly; and second, the simulation must be computationally efficient. As the foot approaches and leaves the ground, its position changes discretely during a numerical integration. At what point during the simulation should a ground spring begin to apply force? An elegant solution to this problem is to use a spring whose force varies exponentially with displacement. Exponential ground springs always apply forces to the feet irrespective of the height of the feet above the ground; however, at some prescribed height the spring forces become negligible. We found that integration time is less when exponential functions are used for the ground springs compared with linear, quadratic, or high-degree polynomials [42–45].

Five spring-damper units are distributed over the sole of each foot in the model. Four spring-damper units are located at the corners of each hindfoot, and one is positioned at the distal end of the toes (Figure 3C). Each spring applies a force in all three directions. The force applied by the ith spring in the vertical direction varies exponentially with the height of the foot above the ground (Figure 4):

$$F_{y_i} = 0.5336\, e^{-1150(p_{y_i} - y_0)} - 1000 v_{y_i}\, g(p_{y_i});$$
$$g(p_{y_i}) = \frac{1}{1 + 10\, e^{500(p_{y_i} - g_0)}}. \quad (1)$$

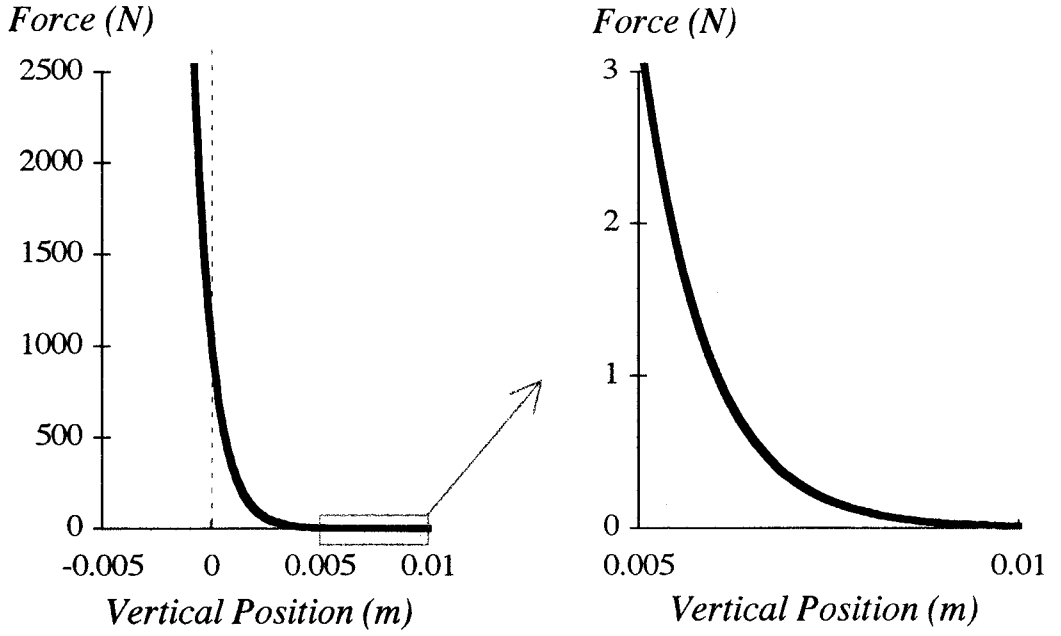

FIGURE 4 Elastic property of the ground springs in the vertical direction. The vertical force applied to the foot by each ground spring is given by equation (1). The curve on the right shows an expanded view of a portion of the curve on the left. Each spring in the model always exerts a force on the foot, but the force quickly becomes negligible as the foot rises above the ground. At 0.01 m above the ground, the vertical force is about 10^{-2} N. At 0.02 m above the ground, the vertical force is less than 10^{-6} N.

Here v_{y_i} is the vertical velocity of the point of application of the spring force; p_{y_i} is the vertical position of the point of application of the spring force; y_0 (0.0065905 m) is a parameter that determines when the magnitude of the spring force becomes significant (i.e., greater than 0.5 N); $g(p_{yi})$ is a function that gradually brings damping into effect as the foot approaches the ground; and g_0 (0.02 m) is a parameter that determines the point at which the damping force is applied.

The forces applied by the ith spring in the fore-aft and transverse directions are each linear functions of the foot position in the transverse plane:

$$F_{x_i} = 6.9 \times 10^4 (p_{x_i} - x_{0_i}) - 1000 v_{x_i} \quad (2)$$

$$F_{z_i} = 6.9 \times 10^4 (p_{z_i} - z_{0_i}) - 1000 v_{z_i}. \quad (3)$$

Here v_{x_i} and v_{z_i} are the velocities of the point of application of the spring force in the fore-aft and transverse directions; p_{x_i} and p_{z_i} are the fore-aft and transverse positions of the point of application of the spring force; and x_{0_i} and z_{0_i} are the free lengths of the spring in each direction. If the magnitude of the force applied in either the fore-aft or transverse direction is larger than that applied in the vertical direction, the foot will slip. New values of x_{0_i} and z_{0_i} are then needed in order to hold F_{x_i} and F_{z_i} at their limiting value of 0.7 F_{y_i}. Because equations (2) and (3) are linear, the required values of x_{0_i} and z_{0_i} can be found by inverting these equations analytically. Note that when the foot is above the ground, horizontal forces are still exerted by the springs, but, since the vertical force is negligibly small, the horizontal forces are also negligibly small and sliding occurs.

The values of the constants in equations (1)–(3) were determined by solving an optimization problem which minimized the number of integration steps needed to simulate the foot-ground interaction. Using these values, a single spring placed under the foot would bring the foot to rest 0.25 mm above the ground when the applied vertical force is 745 N (approximately body weight). When the applied vertical force is 1862 N (2.5 times body weight), which is approximately the peak force generated during jumping, a single spring placed under the foot would bring the foot to rest 0.5 mm *below* the ground. Since five springs act under each foot, total penetration of the feet into the ground will be much less than 0.5 mm during a maximal vertical jump.

Model Anthropometry

Anthropometric measurements were made on each of the five male subjects who participated in this study (age 26 ± 3 yr, height 177 ± 3 cm, and weight 70.1 ± 7.8 kg). All data were recorded according to the methods described by McConville *et al.* [46]. The mass, position of the center of mass, and principal moments of inertia for each segment in the model, except the hindfeet and toes, were calculated by averaging the anthropometric data for the subjects (Table II). Because the geometry of the muscles in the model was based on data reported by Delp [47], the lengths of the body segments were also taken from that study.

For the hindfoot and toes, the mass, position of the center of mass, and moments of inertia were found by representing the volume of each segment by a set of interconnected vertices, the coordinates of which were derived by measuring the surface of a size 10 tennis shoe (Figure 3). Assuming a uniform density of 1.1 gm/cm^3 for the feet [48], the density was numerically integrated over the volume of each segment (see Anderson [26] for details). The combined mass of the hindfoot and toes in the model is similar to the mass of the whole foot reported by McConville *et al.* [46] plus the mass of a size 10 tennis shoe.

Model of the Ligaments

To prevent the joint angles in the model from reaching values which are physically impossible, joint torques are applied to simulate the action of the ligaments. Ligament torques are computed as the sum of two exponential terms [49]:

$$T_{lig_j} = k_{0_j} + k_{1_j} e^{k_{2_j}(q_j - \theta_j)} + k_{3_j} e^{k_{4_j}(q_j - \phi_j)}. \quad (4)$$

Here T_{lig_j} is the net ligament torque applied about the jth joint ($j = 7, 23$); q_j is the angular displacement of the jth joint; and $k_{0_j}, k_{1_j}, k_{2_j}, k_{3_j}, \theta_j$, and ϕ_j are constants which determine the shape of the

ligament torque-angle curve. The values of these constants are given by Anderson [26].

Segments which have small masses such as the metatarsals introduce numerical instabilities during a forward integration of the model. To increase the numerical stability of the model, a damping torque (T_{damp_j}) was applied at each joint:

$$T_{damp_j} = -\eta \dot{q}_j, \tag{5}$$

The constant η (10^{-3} Nms) is the damping coefficient that determines the magnitude of the applied torque. Compared with the torques produced by the muscles, very small damping torques are needed to stabilize the model. For example, even if the angular velocity of a joint was as high as 10 rad/sec (570 deg/sec), the torque due to damping would be only 0.01 Nm, which is several orders of magnitude lower than the torques applied by the muscles.

Musculotendon Dynamics

Each actuator is modeled as a three-element muscle in series with tendon (Figure 5) (see Zajac [50] for a review). The force-producing characteristics of an actuator depend on the maximum isometric strength of the muscle (F_o^m) and its corresponding fiber length (l_o^m) and pennation angle (α), the maximum shortening velocity of muscle ($v_{\max}^m$), and the rest length of the tendon (l_s^T). A single, nonlinear, differential equation defines the relationship between the time rate of change of musculotendon force ($\dot{F}^{MT}$) and musculotendon length (l^{MT}), musculotendon velocity (v^{MT}), and muscle activation (a) [5]:

$$\dot{F}^{MT} = f\left(F^{MT}, l^{MT}, v^{MT}, a\right);\ 0.01 \leq a \leq 1 \tag{6}$$

Given the instantaneous values of F^{MT}, l^{MT}, v^{MT} and a, the force developed by the actuator at the next time instant is found by numerically integrating equation (6).

Excitation-Contraction Dynamics

Muscle cannot be activated or relaxed instantaneously. This behavior is explained partly by the force-velocity property of muscle, but it is also a

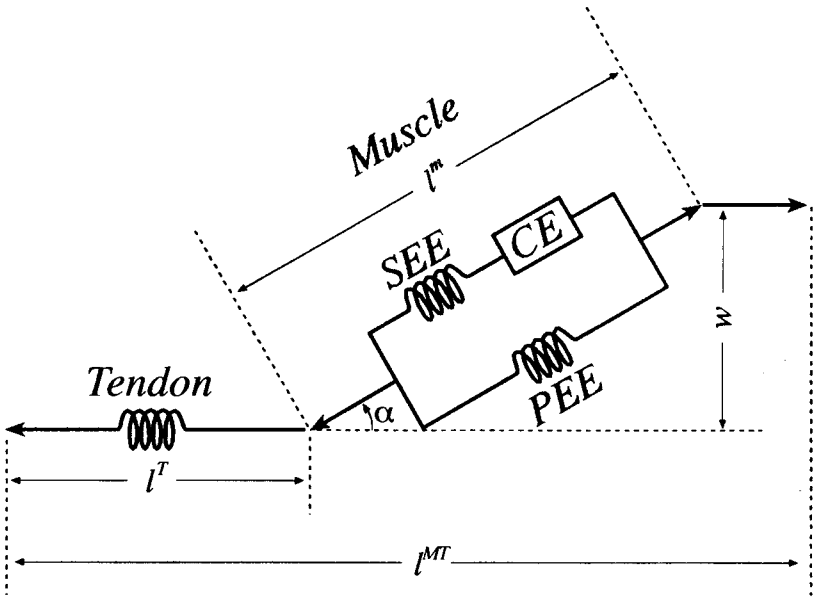

FIGURE 5 Schematic of the musculotendon model used in this study. The mechanical behavior of muscle is described by a Hill-type contractile element (CE), a series-elastic element (SEE), and a parallel-elastic element (PEE). The stress-strain curve for tendon is assumed to be linear. The instantaneous length of the actuator (l^{MT}) is determined by the instantaneous length of the muscle (l^M), the instantaneous length of the tendon (l^T), and the pennation angle of the muscle (α). Note that the width of the muscle (w) remains constant as muscle length changes. (From Zajac [50]).

result of the time course of muscle activation. A first-order differential equation relates the time rate of change of muscle activation ($\dot{a}$) to muscle excitation (u) [51]:

$$\dot{a} = (1/\tau_{rise})(u^2 - ua) + (1/\tau_{fall})(u - a);$$
$$u = u(t); \quad a = a(t) \tag{7}$$

The parameters τ_{rise} and τ_{fall} are the rise and decay time constants associated with muscle activation. We assumed values of 22 and 200 msec for τ_{rise} and τ_{fall}, respectively [50].

Musculoskeletal Geometry

The paths of the muscles are based on geometric data (i.e., musculotendon origin and insertion sites) reported by Delp [47]. In all cases, tendon is assumed to attach at a point to bone. Wherever possible, an entire muscle group is modeled as a single actuator (e.g., biceps femoris long head, semimembranosus, and semitendinosus are combined into HAMS) (see Table III and Figure 1). Many of the smaller muscles which span the ankle are grouped into one of four muscles: PFIN, PFEV, DFIN, and DFEV. Gluteus maximus and gluteus medius/minimus, which have fan-like origins on the pelvis, are each split into two muscles.

The path of each actuator is represented either by a series of straight lines or by a combination of straight lines and space curves from origin to insertion. Straight-line segments are used whenever an actuator can run freely from one point to another, with intermediate or *via points* introduced to model contact of the muscle with bony prominences. *Via cylinders* are used to model the path of a muscle when the muscle wraps completely around the underlying bone and/or other muscles. By using a via-cylinder rather than a series of via-points, muscle moment arms at some of the joints can be represented more accurately. Five via cylinders are used to represent the paths of some of the muscles spanning the hip and the knee: two via cylinders model wrapping of GMAXL and GMAXM around the ischium; one via cylinder models wrapping of ILPSO around the public ramus; one via cylinder models wrapping of HAMS around the medial and lateral condyles of the femur; and one via cylinder models wrapping of GAS around the medial and lateral condyles of the femur. The parameters defining the geometry of the via cylinders at the hip are based on the via points for gluteus maximus and iliopsoas reported by Delp [47]. The parameters for the via cylinders at the knee were estimated by inspecting MR images of the hamstrings and gastrocnemius muscles reported by Reicher [52].

Musculotendon Properties and Strength Scaling

For each actuator, the values of F_o^m, l_o^m, α, and l_s^T were based on data reported by Delp [47] (Table III). When separate muscles were combined and represented as a single muscle (e.g., tibialis posterior, flexor digitorum longus, and flexor hallucis longus), or when the separate portions of a muscle were lumped into one muscle (e.g., medial and lateral heads of gastrocnemius), the values of the musculotendon parameters were estimated by calculating a strength-weighted average of the values reported for the separate muscles. The maximum shortening velocity of all muscles was assumed to be $v_{\max}^m = 10 l_o^m$ ms^{-1}. This value was chosen to model the presence of mixed fiber-type muscles throughout the body [50].

The strengths of the muscles in the model were scaled using measurements of muscle strength obtained from each of the five subjects. A Biodex dynamometer was used to measure the net extensor and flexor torques developed at the hip, knee, and ankle and the net abduction and adduction torques developed at the hip during maximum, voluntary, isometric contractions of the muscles. The values of F_o^m reported by Delp [47] were then adjusted so that the maximum isometric torques for the model matched the average values measured for the subjects. Maximum isometric torques could not be measured for the back; therefore, the values of F_o^m for the back muscles were scaled using experimental data reported in the literature. Since tendon rest

TABLE III Values of the maximum isometric strength of each muscle (F_o^m), optimal muscle-fiber length (l_o^m), muscle pennation angle (α), and tendon slack length (l_s^T) assumed in the model. Actuators on the left and right sides of the body are assumed to have the same parameter values

	Actuator	F_o^m [N]	l_o^m [m]	l_s^T [m]	α [deg]
FDH	flexor digitorum longus/brevis flexor hallucis longus/brevis	1184	0.0400	0.3900	8
EDH	extensor digitorum longus/brevis extensor hallucis longus/brevis	760	0.1100	0.3200	7
DFIN	tibiablis anterior extensor hallucis longus	1003	0.1050	0.2600	5
DFEV	peroneus tertius extensor digitorum	609	0.1000	0.3000	9
PFIN	tibialis posterior flexor digitorum longus flexor hallucis longus	2149	0.0400	0.3700	10
PFEV	peroneus brevis peroneus longus	1556	0.0500	0.3000	7
SOL	soleus	3016	0.0500	0.2540	25
GAS	gastrocnemius	1651	0.0600	0.3950	17
BFSH	short head of biceps femoris	681	0.1730	0.0500	23
VAS	vastus medialis, intermedius, lateralis	6865	0.0870	0.1400	3
RF	rectus femoris	1320	0.1140	0.3200	5
HAMS	semimembranosus semitendinosus biceps femoris	2814	0.1090	0.3400	8
GRA	gracilis	183	0.3520	0.1350	3
TFL	tensor fasciae latae	262	0.0950	0.4250	3
SAR	sartorius	176	0.5790	0.0400	0
GMAXL	lateral gluteus maximus	1730	0.1450	0.1060	2
GMAXM	medial gluteus maximus	686	0.1540	0.1200	5
GMEDA	anterior gluteus medius anterior gluteus minimus	1319	0.0653	0.0551	4
GMEDP	posterior gluteus medius posterior gluteus minimus	1215	0.0650	0.0484	7
ADM	adductor magnus	1245	0.1210	0.1200	4
ADLB	adductor longus brevis	994	0.1280	0.0420	6
ILPSO	iliopsoas	1627	0.1040	0.1350	8
PECT	pectinius	301	0.1330	0.0010	0
PIRI	piriformis	502	0.0300	0.1020	10
ERCSPN	erector spinae	2974	0.1200	0.0300	0
INTOBL	internal obliques	712	0.1250	0.1650	0
EXTOBL	external obliques	864	0.1250	0.2110	0

lengths cannot be determined experimentally, these parameters were estimated in the model. The values of l_s^T reported by Delp [47] were adjusted until the shapes of the torque-angle curves for the model were consistent with those obtained from experiment (see Appendix).

Body-Segmental Dynamics

The dynamical equations of motion for the 10-segment, 23 dof, 54-muscle model may be expressed as:

$$A(\underline{q})\ddot{\underline{q}} + B(\underline{q})\dot{\underline{q}}^2 + C(\underline{q}) + M(\underline{q})\underline{F}^{MT} + \underline{T}_{lig}(\underline{q}, \dot{\underline{q}}) + \underline{T}_{foot}(\underline{q}, \dot{\underline{q}}) = \underline{0} \quad (8)$$

where $\underline{q}$, $\dot{\underline{q}}$, and $\ddot{\underline{q}}$ are 23×1 vectors of joint-angular displacements, velocities, and accelerations; $A(\underline{q})$ is the 23×23 system mass matrix; $B(\underline{q})\dot{\underline{q}}^2$ is a 23×1 vector of Coriolis and centripetal terms; $C(\underline{q})$ is a 23×1 vector of gravitational forces; $M(\underline{q})$ is a 23×54 matrix containing the muscle moment arms; $\underline{F}^{MT}$ is a 54×1 vector of musculotendon forces; $\underline{T}_{lig}(\underline{q}, \dot{\underline{q}})$ is a 23×1 vector of ligament and damping torques; and $\underline{T}_{foot}(\underline{q}, \dot{\underline{q}})$ is a 23×1 vector containing the spring forces used to model the interaction between the feet and the ground. Equation (8) comprises a set of 23 second-order, nonlinear, differential equations. These equations were derived in symbolic form using a commercial software package called SD/Fast [53].

NUMERICAL SIMULATION

A direct-dynamics approach was used to simulate jumping. The dynamical equations of motion (equations (6)–(8)) may be written in the form

$$\dot{\underline{x}} = f(\underline{x}, \underline{u}, t) \quad (9)$$

where the state vector, $\underline{x} = \{\underline{q}, \dot{\underline{q}}, \underline{F}^{MT}, \underline{a}\}^T$, is composed of 154 elements: 23 joint-angular displacements ($\underline{q}$); 23 joint-angular velocities ($\dot{\underline{q}}$); 54 musculotendon forces ($\underline{F}^{MT}$); and 54 muscle activations ($\underline{a}$). The control vector ($\underline{u}$) contains the muscle excitations and is also composed of 54 elements. Given the values of the initial states ($\underline{x}_0 = \underline{x}(0)$) and the time histories of the muscle excitations ($\underline{u}$), the time histories of the resulting muscle activations ($\underline{a}$), musculotendon forces ($\underline{F}^{MT}$), and body-segmental motions ($\underline{q}, \dot{\underline{q}}, \ddot{\underline{q}}$) can be found by integrating equation (9) forwards in time. Numerical integration was performed using a Runge-Kutta-Feldberg 5–6 variable-step integrator. Approximately 4000 time steps were needed to simulate jumping in three dimensions. The muscle excitations needed to produce a maximal vertical jump were found by applying dynamic optimization theory [54].

DYNAMIC OPTIMIZATION PROBLEM

For vertical jumping, the goal is to maximize the height reached by the center of mass of the body,

$$J = Y_{cm}(t_f) + \dot{Y}_{cm}^2(t_f)/2g, \quad (10)$$

where $Y_{cm}(t_f)$ is the vertical position of the whole-body center of mass, evaluated at the instant of lift-off, t_f; $\dot{Y}_{cm}(t_f)$ is the vertical velocity of the whole-body center of mass at lift-off; and g is the value of gravitational acceleration on Earth (9.81 ms^{-2}). To prevent joint hyperextension in the model, a penalty function (ϕ) was added to the performance criterion (J) in equation (10):

$$\phi = w \int_0^{t_f} \left[\sum_{j=1}^{17} T_{lig_j}^2 \right] dt \quad (11)$$

where w (0.001) is a parameter that weights the value of the penalty function against the value of the performance criterion, and T_{lig_j} is the torque applied by the ligaments at the jth joint. Thus, the dynamic optimization problem can be stated as follows: maximize jump height (equation (10)) subject to the dynamical equations of motion (equation (9)) and the penalty function (equation (11)) which prevents joint hyperextension during the jump.

OPTIMIZATION OF INITIAL CONDITIONS

At time $t = 0$, the model is in a squatting position, at rest, and in static equilibrium (i.e., the velocities and accelerations of all the generalized coordinates are zero). Since the velocities of the generalized coordinates are states in the model (see equation (9)), these quantities can be set to zero initially. The accelerations, however, are generated by the joint torques and external forces applied to the model. Therefore, an appropriate set of muscle forces (or muscle activations) and ground-spring forces must be applied in order to hold the model in static equilibrium. Since the number of muscle activations and ground-spring forces is greater than the number of dof's of the model, optimization theory was used to solve for the muscle activations and ground-spring forces needed to keep the model in static equilibrium.

The vertical ground-spring forces depend on the height of the foot relative to the ground, which in turn depends on the position and orientation of the pelvis and the joint-angular displacement of each hip, knee, ankle, and metatarsal joint. The ground-spring forces cannot be treated as independent variables in the optimization problem because these quantities are a function of the generalized coordinates. If the configuration of the body in the squatting position could be determined accurately enough for the subjects, then this configuration could also be used in the model. Unfortunately, this is not possible for two reasons. First, video-based, kinematic systems cannot record the displacements of the body segments accurately enough, and changes of the order of 0.1 mm can cause large changes in the forces exerted by the ground springs. Second, the model and the subject anthropometry are not identical.

Alternatively, it is possible to control the height of each foot relative to the ground by adjusting the values of some of the generalized coordinates in the model, specifically, the vertical displacement of the pelvis (q_2), pelvic tilt (q_6), the subtalar joint angles (q_{15} and q_{22}), and the metatarsal joint angles (q_{16} and q_{23}). The values of the remaining generalized coordinates were set equal to the average values of the corresponding generalized coordinates measured for the subjects. Thus, the parameter optimization problem for the initial conditions can be stated as: find the values of the generalized coordinates (q_2, q_6, q_{15}, q_{22}, q_{16}, and q_{23}) and the values of the muscle activations ($a_i; i = 1, 54$) such that muscle "effort" is minimized and the acceleration of each generalized coordinate is zero.

Solving for the values of the generalized coordinates and the muscle activations simultaneously proved to be numerically infeasible. Instead, these quantities were calculated by solving two separate optimization problems. In the first problem, the values of the generalized coordinates, q_2, q_6, q_{15}, q_{22}, q_{16}, and q_{23} were found by minimizing the sum of the squares of the joint torques,

$$J = \sum_{i=7}^{23} T_i^2, \tag{12}$$

subject to the constraint that the accelerations of all the generalized coordinates remain zero,

$$C(\underline{q}) + \underline{T}_{mus}(\underline{q}) + \underline{T}_{lig}(\underline{q}) + \underline{T}_{foot}(\underline{q}) = \underline{0}. \tag{13}$$

Here $\underline{T}_{mus}(q)$ is a 23×1 vector containing the net joint torques due to the muscles, and all other terms are defined in equation (8) above. Note that $\underline{T}_{mus}(\underline{q})$ can be found uniquely. Equation (12) was chosen as the cost function because it is assumed that the subjects will position their bodies in the squatting position such that muscle "effort" is minimized. Note also that the generalized coordinates for the pelvis ($i = 1, 6$) are not included in equation (12) because no external forces or torques are applied to the pelvis.

Using the values of the generalized coordinates, q_2, q_6, q_{15}, q_{22}, q_{16}, and q_{23}, obtained from a solution to the above problem (see Table IV), the values of the muscle activations ($a_i; i = 1, 54$) were then found by minimizing the sum of the normalized muscle forces squared,

$$J = \sum_{i=1}^{54} (F_i^{MT}/F_{oi}^m)^2, \tag{14}$$

TABLE IV Initial conditions for the simulated squat jump. The initial value of the generalized coordinate for each joint is given either in meters or degrees. All values, except those denoted by †, were determined by averaging kinematic data obtained from the five subjects. The values denoted by † were obtained using the methods described in the text. θ_k is the knee-joint angle; θ_a is the ankle-joint angle; θ_s is the subtalar-joint angle; and θ_m is the metatarsal-joint angle

Joint	Generalized Coordinate		
pelvis	$x = 0.0$ m†	$y = 0.7805$ m†	$z = 0.0$ m†
	$\theta_x = 0.0°$†	$\theta_y = 0.0°$†	$\theta_z = -25.0°$†
back	$\theta_z = -10.0°$	$\theta_x = 0.0°$†	$\theta_y = 0.0°$†
right hip	$\theta_z = 76.7°$	$\theta_x = -6.0°$	$\theta_y = 3.0°$
right knee	$\theta_k = -80.3°$		
right ankle	$\theta_a = 28.5°$	$\theta_s = 2.596°$†	
right metatarsal	$\theta_m = -0.31°$†		
left hip	$\theta_z = 76.7°$	$\theta_x = -6.0°$	$\theta_y = 3.0°$
left knee	$\theta_k = -80.3°$		
left ankle	$\theta_a = 28.5°$	$\theta_s = 2.596°$†	
left metatarsal	$\theta_m = -0.31°$†		

subject to the constraint that the accelerations of all the generalized coordinates remain zero (equation (13)). In equation (14), F_i^{MT} is the force developed by the ith actuator and F_{oi}^m is the peak isometric force in the ith muscle. The parameter optimization problems described in this section were solved using a gradient-based algorithm reported by Powell [55].

COMPUTATIONAL ALGORITHM

The pattern of muscle excitations which produces a maximal vertical jump was found by converting the dynamic optimization problem into a parameter optimization problem [51]. In this approach, each muscle excitation history is discretized into a set of independent variables or *control nodes*. The parameter optimization problem is to find the values of the control nodes which produce the highest possible jump. Once the values of the control nodes are known, each muscle excitation history is reconstructed using linear interpolation (Figure 6). Sixteen control nodes were used to represent the excitation history for each muscle in the model. Therefore, the total number of unknown variables in the parameter optimization problem is $54 \times 16 = 864$. To reduce the size of the problem, we assumed that the muscle excitation histories for each side of the body are identical during a maximal vertical jump. This assumption reduced the number of unknown variables by a factor of two to 432.

A single iteration of the computational algorithm comprises three steps (Figure 7): (1) a nominal forward integration of the dynamical equations to evaluate the performance criterion and the constraints; (2) execution of a series of *perturbed* forward integrations to evaluate the first derivatives of the performance criterion and constraints with respect to each control node; and (3) execution of an optimization routine to find a new set of control nodes which improves the values of the performance criterion and/or constraints. The most significant feature of this algorithm is that its structure is very well suited to the architecture of a parallel computer. The reason is that each perturbed forward integration in step 2 can be performed *independently*.

The computational algorithm was executed on three types of Multiple Instruction, Multiple Data (MIMD) parallel computers housed at the NASA-Ames Research Center in California: an Intel iPSC/860 (Intel), a Connection Machine 5 (CM-5), and an IBM SP-2 (SP-2). Each machine combines a

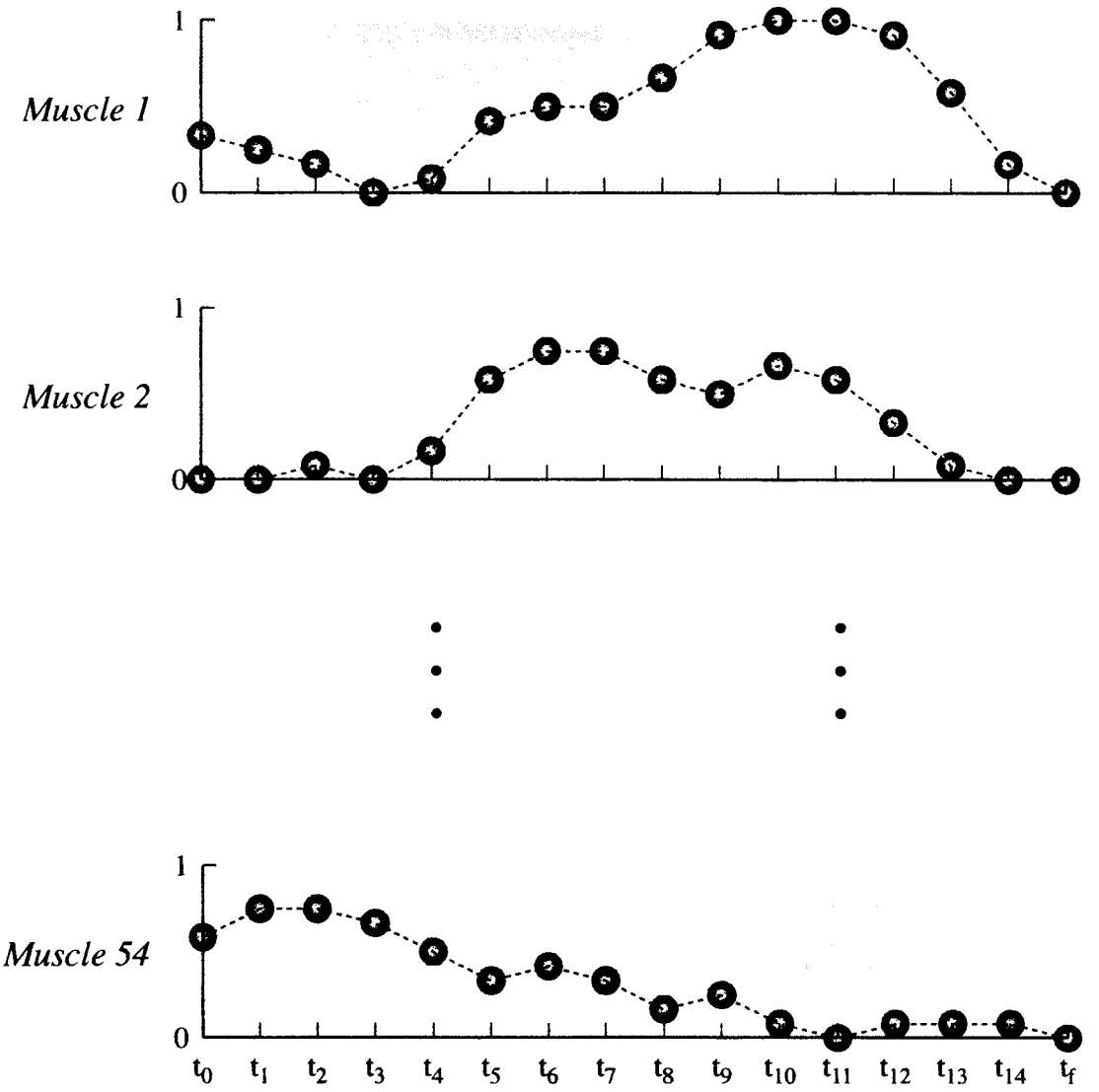

FIGURE 6 Schematic showing the excitation histories of the muscles in the model. The time history of each muscle excitation is discretized to form 16 independent control nodes. Parameter optimization is then used to calculate the values of the control nodes.

number of separate processors into a sophisticated communication network: the Intel has 128 processors; the CM-5 has 512 processors; and the SP-2 has 160 RS 6000/590 processors.

EXPERIMENTS

Each of the five subjects performed five maximal vertical jumps. Each jump began with the subject positioned in a static squat. The depth of the squat was fixed by requiring shoulder height to be 80% of its value at standing. The subject moved into the prescribed position by viewing himself on a large-screen television monitor. To eliminate arm swing, the jump was executed with the arms crossed over the chest.

EMG, force-plate, and kinematic data were recorded simultaneously during each jump. The vertical, fore-aft, and transverse components of the

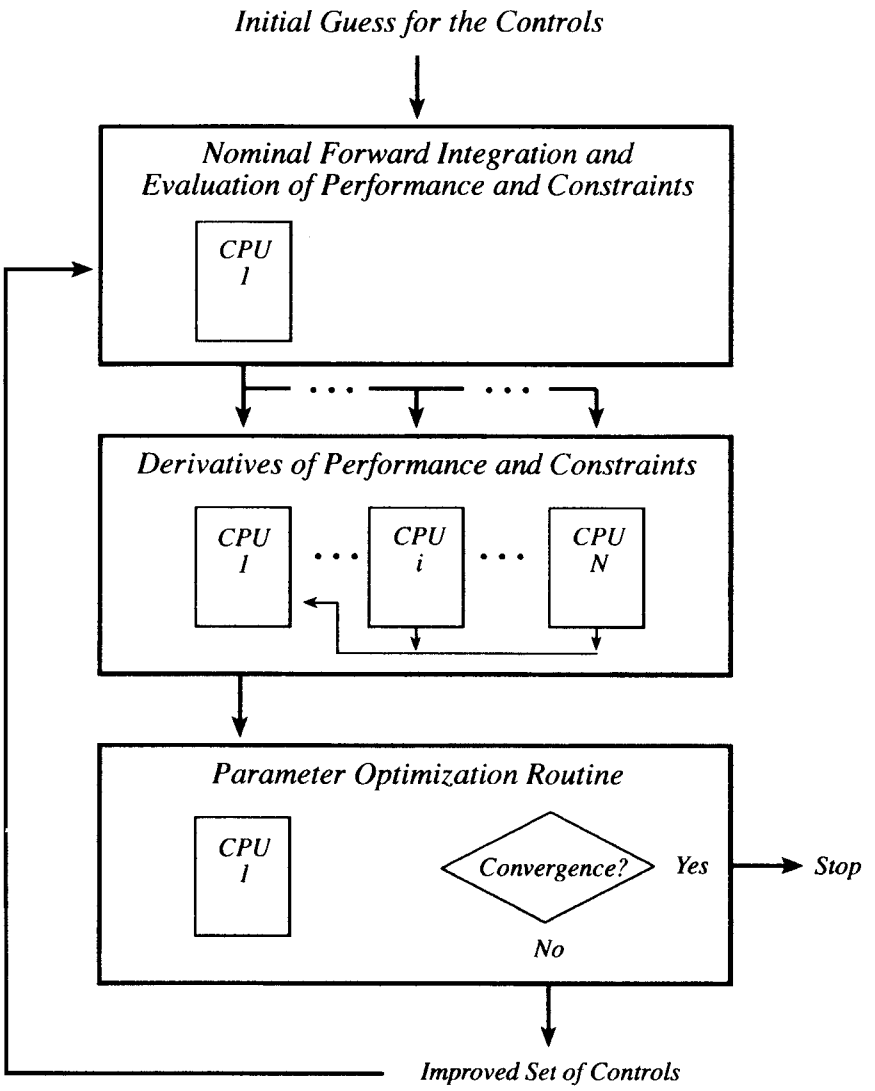

FIGURE 7 Flowchart illustrating the general structure of the computational algorithm. Computation of the derivatives of the performance criterion and constraints consumes over 90% of the CPU time needed for each iteration of the algorithm. Great savings in total CPU time can be obtained by using a parallel computer to calculate the derivatives.

resultant ground-reaction force were measured using a six-component, strain-gauged transducer. EMG data were recorded using surface electrodes mounted over the following muscles on the right side of the body: tibialis anterior, soleus, lateral gastrocnemius, vastus lateralis, rectus femoris, hamstrings, adductor magnus, gluteus maximus, gluteus medius, erector spinae, and the external abdominal obliques.

The three-dimensional positions of markers mounted on the subject's body were measured using a four-camera, passive-marker, video-based system. Three markers were used to determine the position and orientation of the pelvis relative to a global (inertial) reference frame fixed on the ground: one marker was placed on the right anterior superior iliac spine, one on the left anterior superior iliac spine, and one on the sacrum. Three markers were also used to determine the orientation of the torso relative to the pelvis: one marker was placed on the right acromion, one on the left acromion, and one

on the spine at the level of the distal borders of the scapulae. Only two markers were mounted on each thigh, shank, and foot. Since the positions the joint centers were known in a local reference frame fixed in each segment, the joint center was used as the third marker for the thigh, shank, and foot. For the thigh, one marker was placed on the vastus medialis, three-quarters of the length of the femur down from the hip; the other marker was placed on the hamstrings, two-thirds of the length of the femur down from the hip. For the shank, one marker was placed on the head of the fibula; the other, on the anterior spine of the tibia, approximately 5 cm above the ankle. For the foot, one marker was placed on the calcaneus; the other, on the distal end of the fifth metatarsal. Because the kinematic methods used in this study are relatively insensitive to marker placement, it was not necessary to place the markers in exactly the same location for each subject. The Euler angles at each joint were calculated using the rotation matrix given by Craig [56].

RESULTS

Computation of the Optimal Solution

About 200 iterations of the computational algorithm were needed to converge to the dynamic optimization solution for jumping. More than 1800 hours (2.5 months) of CPU time are needed to solve the problem using a 180 MHz MIPS R5000 Silicon Graphics Indigo. If a much faster serial machine such as the IBM RS/6000 is used, CPU time is reduced by more than a factor of two (Figure 8). Even greater savings are obtained when the derivatives of the performance criterion are evaluated using a parallel computer. The optimal solution for jumping can be found with 324 hours of CPU time on the Intel, 286 hours of CPU time on the CM-5, and 23 hours of CPU time on the SP-2 (Figure 8). The reason for the speed-up on the parallel machines is that the calculation of the derivatives can be distributed across multiple processors (Figure 7, Step 2). Even

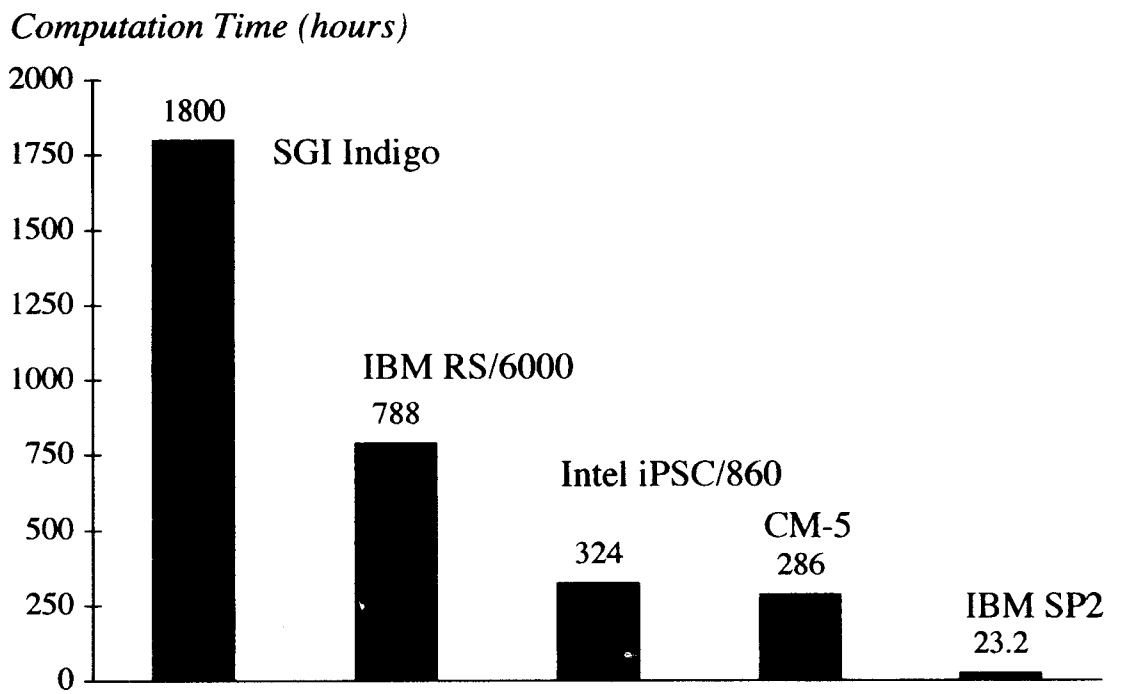

FIGURE 8 Computation time needed to solve the dynamic optimization problem for jumping using the three-dimensional, musculoskeletal model developed in this study. Both the SGI and IBM RS/6000 are serial workstations; the Intel iPSC/860, the CM-5, and the IBM SP2 are parallel supercomputers. The estimates for the parallel machines assume that 128 processors are used to compute the derivatives.

though the derivatives can be computed over 100 times faster on the parallel computers, the time taken to complete one full iteration of the algorithm is limited by the time taken to execute the parameter optimization routine, which at present can be run on only one processor (Figure 7, Step 3).

Comparison of Model and Experiment

There is quantitative agreement between the response of the model and the way each of the five subjects executed a maximal vertical jump. EMG data recorded for each subject indicate a stereotypic pattern of muscle coordination: the back, hip, and knee extensors (ERCSPN, GMAX, ADM, and VAS) are activated at the beginning of the jump, and the more distal ankle plantarflexors (SOL and GAS) are activated later (Figure 9). Although the model reproduces this behavior, minor differences are also evident between the model predictions and the experimental results. In the model, hamstrings is activated at the beginning of the jump and rectus femoris is activated much later. The subjects, however, chose to activate these muscles at approximately the same time shortly after the start of the jump (cf. thick and thin lines for RF and HAMS). There is also some discrepancy between model and experiment near lift-off. The subjects continue to activate their quadriceps until lift-off, whereas the model chose to de-activate this muscle before leaving the ground (Figure 9, VAS).

In spite of the small differences in muscle coordination, there is excellent agreement between the ground-reaction forces predicted by the model and those generated by the subjects. Peak vertical ground forces measured for the subjects range from 1500 to 2100 N, compared with a peak force for the model of 2000 N (Figure 10, Vertical). The model and the subjects generated much smaller forces in the fore-aft direction: the peak fore-aft components measured for the subjects range from 120 to 270 N, compared with a value of 270 N calculated for the model (Figure 10, Fore-aft). It is significant that the model is able to reproduce the correct pattern for the fore-aft ground-reaction force in view of the fact that previous models of jumping could not (e.g., Pandy and Zajac [57]). This difference may be due to the addition of a back joint and the metatarsal joints in the current model.

The peak vertical acceleration of the whole-body center of mass for the model was 19 m/s^2, which is within the range of values obtained from experiment (15 to 19 m/s^2; Figure 11, Acceleration). The vertical velocity of the whole-body center of mass at lift-off for the model was 2.3 m/s, compared with the range of 2.0 to 2.5 m/s measured for the subjects (Figure 11, Velocity). As a result, the model and the subjects jumped to about the same height; jump height for the model was 36.9 cm, which is very close to the mean of 37 cm measured for the subjects (Table V). One difference between model and experiment, however, is the time to lift-off: the model took 0.26 secs to leave the ground, which is considerably shorter than the average time of 0.30 secs recorded for the subjects.

The model extended its back by 15° prior to lift-off, which is consistent with the range of values recorded for the subjects (cf. thick and thin lines in Figure 12A). The pelvis also tilted at about the same rate and by about the same amount prior to lift-off (Figure 13A). Since the muscle excitation histories were assumed to be identical for each side of the body in the model, the pelvis did not rotate in either the frontal or the transverse plane. The subjects, however, tilted and internally rotated their pelves by as much as 10° during the jump (thin lines in Figure 13B and C).

Compared to the subjects, the model over-extended its hips, knees, and ankles before leaving the ground (cf. thick and thin lines in Figures 14A, 15A and 15B at $t = 0$). We hypothesize that this discrepancy is due to the value assumed for the rise time for muscle activation. The model assumes that the delay between muscle excitation and muscle activation is only 22 msec [50]; however, this value is based on the response of a single muscle fiber, and the results of some experimental studies suggest that the activation rise time for a whole muscle is significantly greater [58]. If the rise time for muscle activation were greater in the model, the

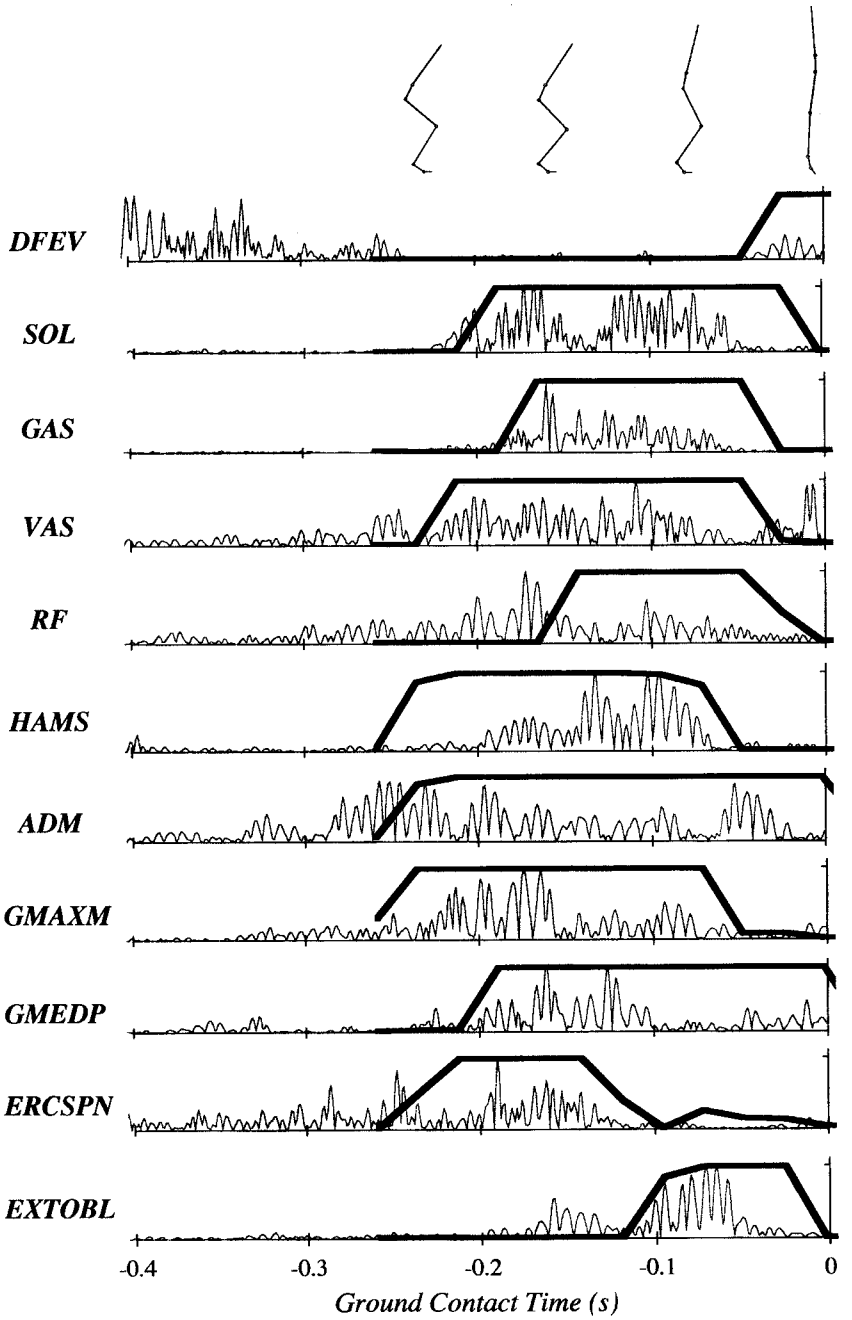

FIGURE 9 Comparison of EMG data recorded for one subject (wavy lines) and the muscle excitation histories predicted by the model (thick lines) for the ground-contact phase of the jump. Subject EMG signals were band-passed between 50 and 200 Hz using an order 100 FIR filter, rectified, and then normalized. Normalization was performed by dividing by the maximum electrode voltage recorded during a maximal contraction or during the jump, whichever was greater. The vertical axes for the model excitations and subject EMG records therefore range from 0 to 1. Time $t = 0$ marks the instant that the model and the subject leave the ground. Muscle abbreviations are defined in Table III. EMG data recorded from tibialis anterior are compared with the excitation history calculated for DFEV in the model; EMG recorded from gluteus maximus is compared with GMAXM in the model; EMG recorded for gluteus medius is compared with GMEDP in the model; and EMG recorded for the abdominal obliques is compared with EXTOBL in the model. The stick figures show the configuration of the model at specific instants during the jump.

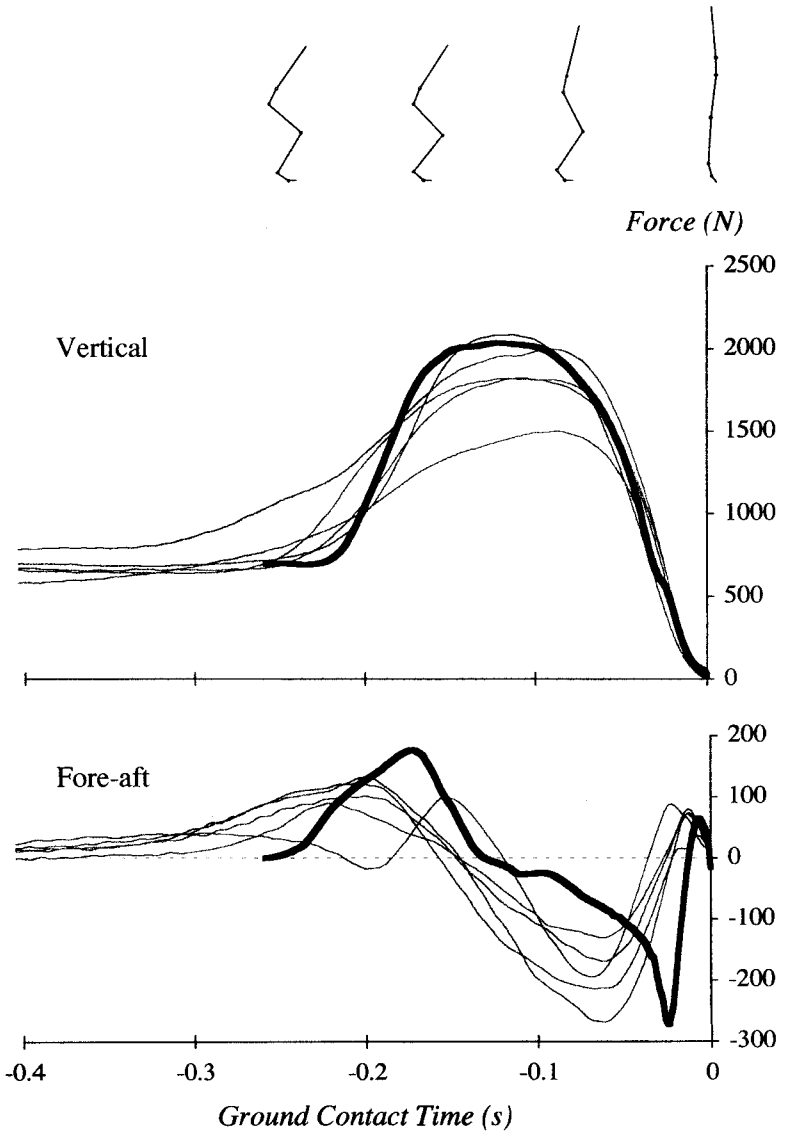

FIGURE 10 Vertical and fore-aft components of the ground-reaction force generated by each of the five subjects (thin lines) and by the model (thick lines) during the ground-contact phase of the jump. For the model, the resultant force in each direction was found by summing the forces developed by the ground springs which act under each foot (see Figure 3C). Time $t = 0$ marks the instant that the model and the subjects leave the ground.

flexor muscles of the knee (e.g., BFSH) would need to turn on earlier to prevent joint hyperextension. Because the knee would then extend more slowly in the model, the rate of hip and ankle extension would also be less. The contention that muscle activation rise time is underestimated in the model is supported by the fact that the model spends less time on the ground than any of the subjects.

DISCUSSION

The model developed in this study is much more detailed than previous models of jumping. In the studies conducted by Pandy *et al.* [5], Pandy and Zajac [57], and Anderson and Pandy [59], the body was modeled as a 4-segment, 4 dof, planar linkage with 8 muscles. Soest *et al.* [6] also represented the

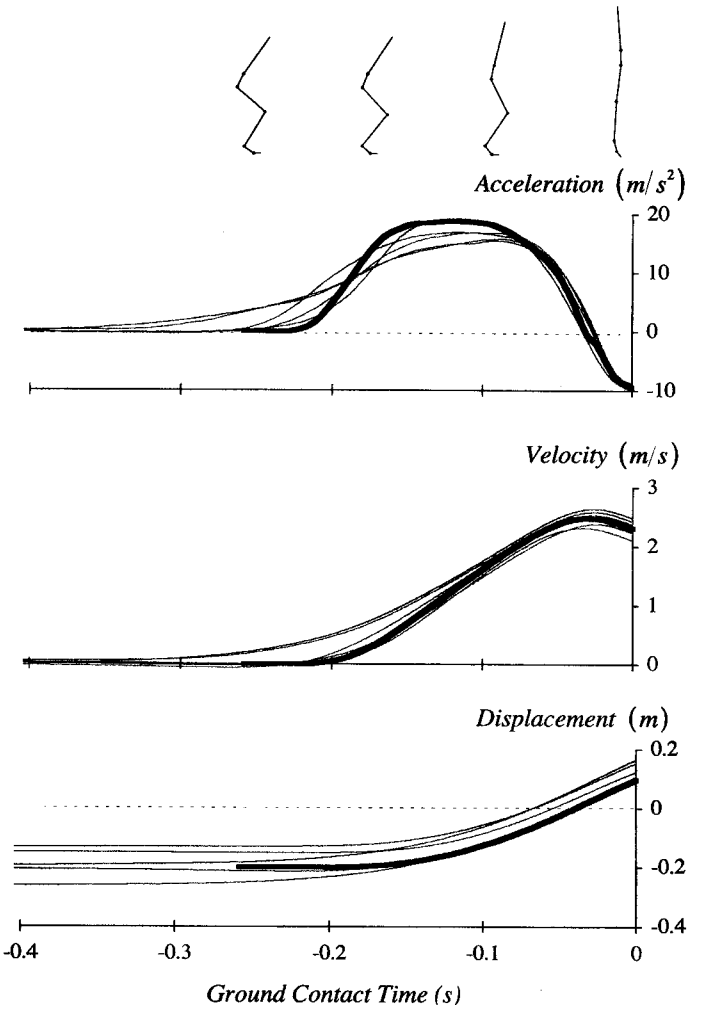

FIGURE 11 Time histories of the vertical acceleration, velocity, and displacement of the center of mass of the whole body for each of the five subjects (thin lines) and for the model (thick lines) during the jump. The vertical acceleration of the center of mass was calculated from the vertical component of the ground-reaction force (Figure 10, Vertical). The vertical velocity of the center of mass was found by integrating the vertical acceleration; and the vertical displacement was found by integrating the vertical velocity. For the model and the subjects, vertical displacement is relative to the height of the center of mass at standing. Standing height is marked by the dashed line in the bottom graph.

TABLE V Comparison of jump height for the subjects and the model. Jump height is the maximum height reached by the center of mass of the body relative to the height of the center of mass at standing. For the subjects, jump height was calculated as the change in the vertical position of the average vertical position of the three pelvic markers. For the model, jump height was calculated using equation (10)

Subject	Jump Height (cm)
1	41
5	40
2	37
3	34
4	33
Model	36.9

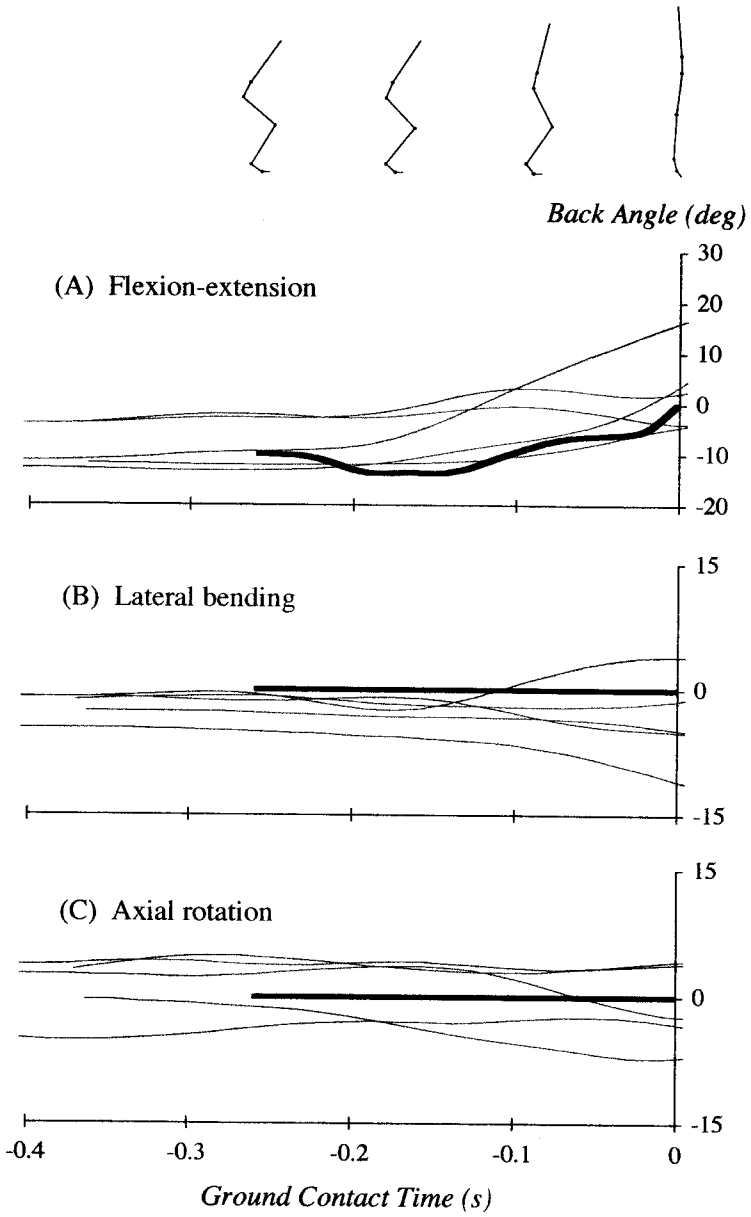

FIGURE 12 Angular displacement of the back for each of the five subjects (thin lines) and for the model (thick lines) during the jump. The back angles define the orientation of the HAT reference frame relative to the pelvis frame and are described by body-fixed ZXY Euler angles (Figure 2). (A) Flexion-extension occurs about the Z axis of the HAT; extension is positive. (B) Lateral bending occurs about the X axis of the HAT; bending to the right is positive. (C) Axial rotation occurs about the Y axis of the HAT; rotation to the left is positive. Time $t = 0$ marks the instant that the model and the subjects leave the ground.

skeleton as a 4-segment, 4 dof, planar linkage, but their model was actuated by only 6 muscles. The interaction between the feet and the ground was also modeled quite simply in each of these studies: the foot was represented as a single link, hinged to the ground at the toes [5,6]. In this study, the body is modeled as a 10-segment, 23 dof linkage, actuated by 54 leg, abdomen, and back muscles. The number of segments is twice the number used in previous models of jumping [5,6]; the number of degrees of

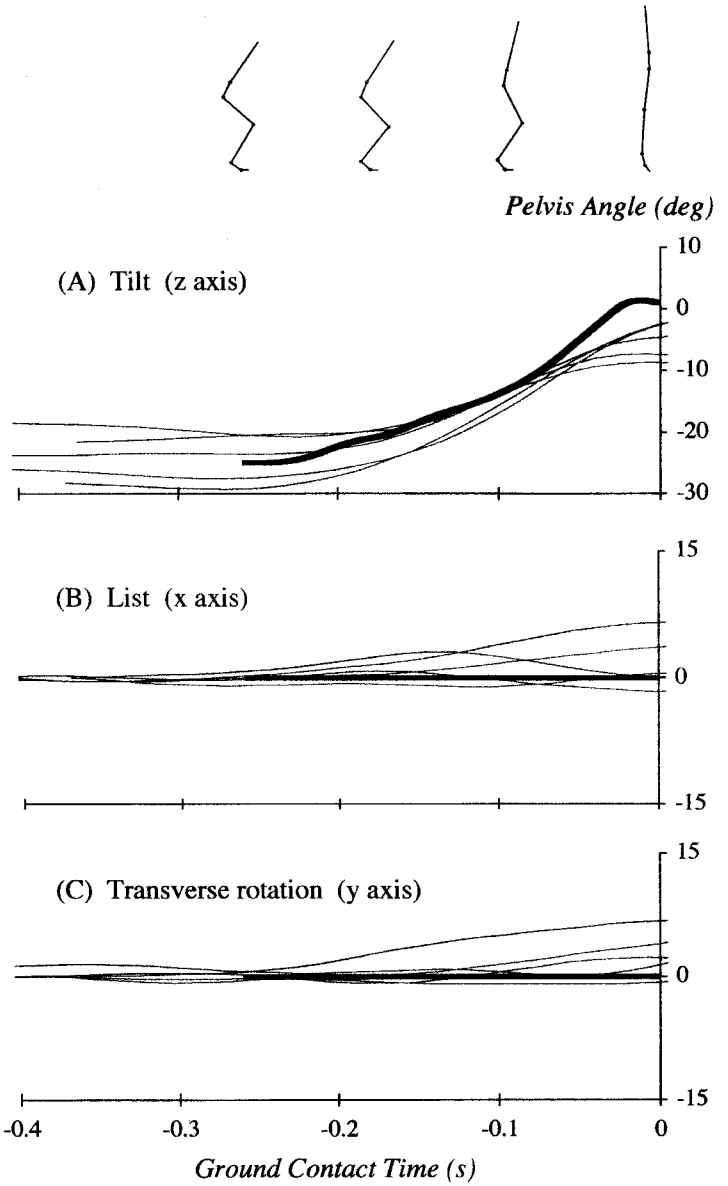

FIGURE 13 Change in orientation of the pelvis reference frame relative to the inertial reference frame (ground) for each of the five subjects (thin lines) and for the model (thick lines) during the jump. The orientation of the pelvis is described by body-fixed XYZ Euler angles (Figure 2). (A) Pelvic tilt occurs about the Z axis of the pelvis; posterior tilt is positive. (B) Pelvic list occurs about the X axis of the pelvis; listing to the right is positive. (C) Transverse rotation occurs about the Y axis of the pelvis; rotation to the left is positive.

freedom is anywhere from 2 to 6 times greater than that considered previously [4,5,10]; the number of muscles is 2 to 5 times greater than that included in previous dynamic optimization models of movement [4,15,60,61]; and the model is free to make and break contact with the ground (Table I).

There are, however, a number of limitations of the model. Although the number of muscles is larger than that considered in previous dynamic optimization studies [2,5,6,17], it is still much less than the number of muscles in the body. Twenty-four muscles actuate each leg in the model, compared with 51

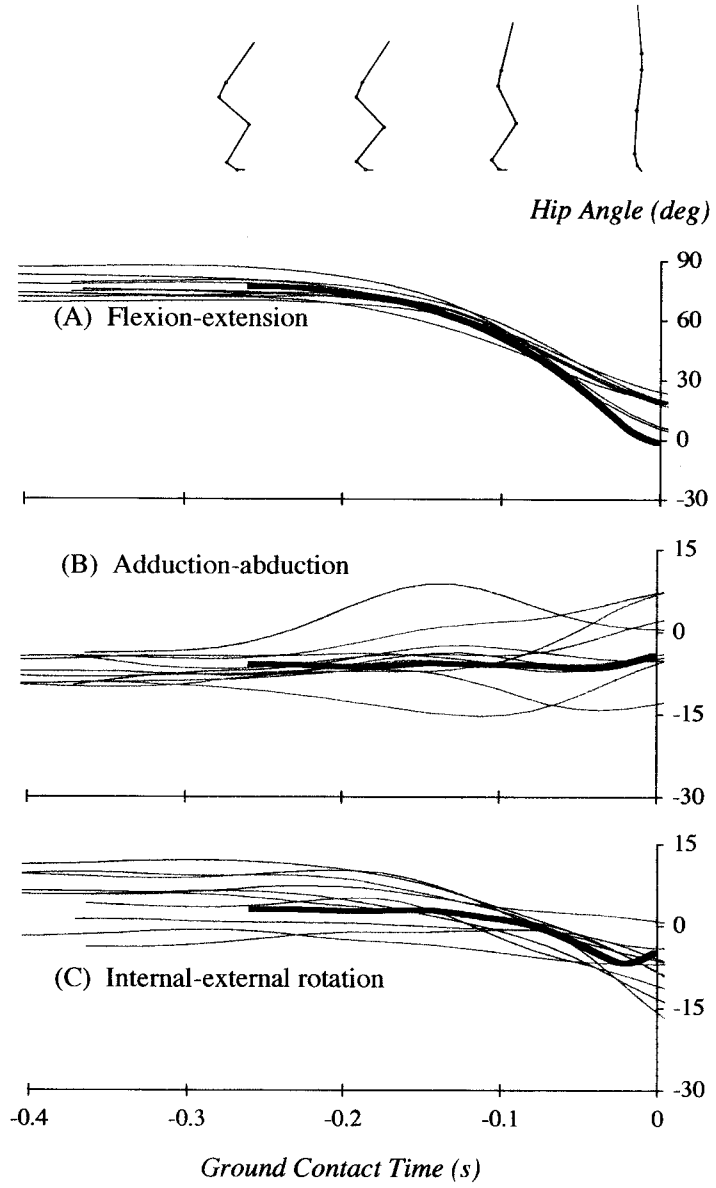

FIGURE 14 Angular displacement of the hip for each of the five subjects (thin lines) and for the model (thick lines) during the jump. The hip angles define the orientation of the thigh relative to the pelvis and are described by body-fixed ZXY Euler angles (Figure 2). For each subject, the trajectories for both hips are plotted. (A) Flexion-extension occurs about the Z axis of the thigh; flexion is positive. (B) Adduction-abduction occurs about the X axis of the thigh; adduction is positive. (C) Internal-external rotation occurs about the Y axis of the thigh; internal rotation is positive. Time $t = 0$ marks the instant that the model and the subjects leave the ground.

muscles in the human leg [62]. The muscles of the trunk are also represented quite simply: 6 abdomen and back muscles control the relative movements of the torso and pelvis in the model, whereas 50 muscles are available to control the movements of the lumbar and thoracic vertebra in the human trunk [62].

The number of muscles included in the model is also less than that considered in many static optimization studies [18,21,63,64]. The reason is

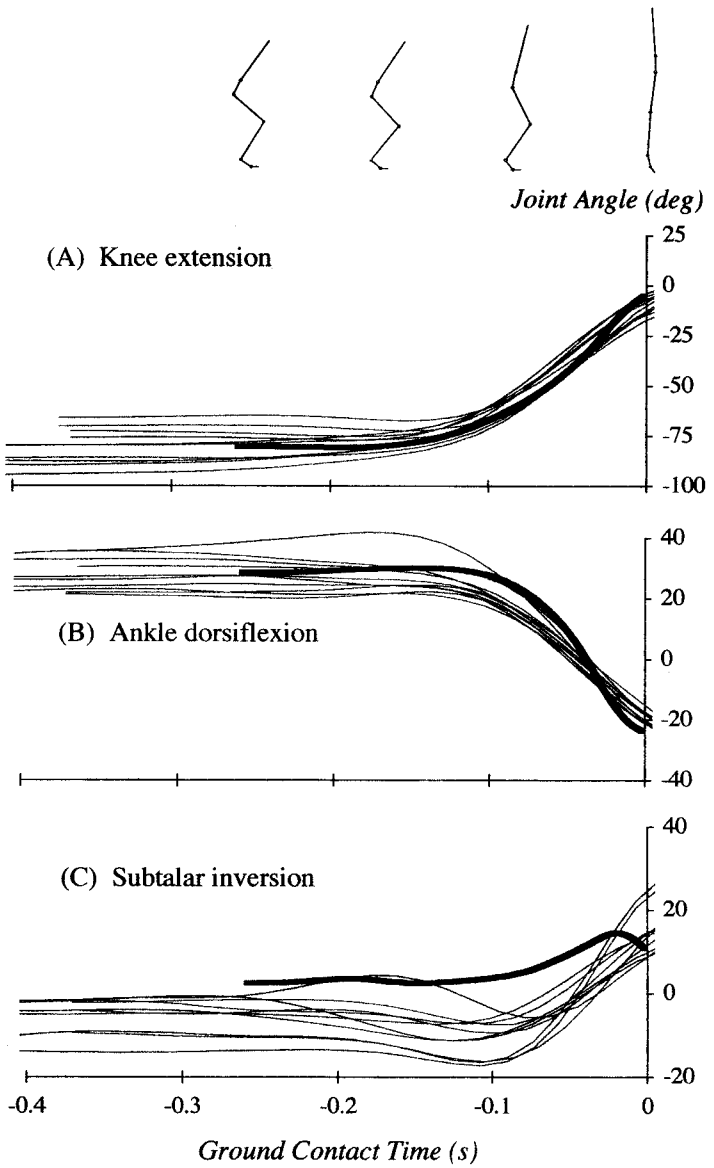

FIGURE 15 Angular displacement of the knee (A), ankle (B), and subtalar joint (C) for each of the five subjects (thin lines) and for the model (thick lines) during the jump. For each subject, the trajectories for both knees, both ankles, and both subtalar joints are plotted. Knee extension, ankle dorsiflexion, and subtalar inversion are all positive. Time $t = 0$ marks the instant that the model and the subjects leave the ground.

that much more computation time is needed to converge to a solution of a dynamic optimization problem compared to the analogous static optimization problem. In fact, as the number of muscles increases, the CPU time needed to solve a dynamic optimization problem increases dramatically [9,12]. Consequently, even with today's fastest parallel machines, some compromise must be made between the complexity of the musculoskeletal model used to represent the body and the computational time needed to simulate movement.

There are also a number of assumptions made in defining the kinematic structure of the model. Perhaps most significantly, the relative movements

of the pelvis and torso are modeled using a single 3 dof back joint, even though the individual vertebrae of the spine move independently of each other in three dimensions [23,24,25,65,66]. The fact that the model accurately reproduces the ground-reaction forces measured during jumping suggests, however, that the relative movements of the vertebrae are less important than the movement of the whole spine in the sagittal plane. The subjects extended their backs anywhere from 10 to 30° prior to lift-off, compared with 15° of back extension predicted by the model (Figure 12A). The abdomen and back muscles were also activated in the same sequence and at approximately the same times in the model and the subjects, which indicates that the muscles represented in the model are those which are most important for extending the back during the propulsion phase of the jump (Figure 9, ERCSPN and EXTOBL).

The axes of rotation at each joint are also assumed to remain fixed in the model. This assumption may be reasonable for the hip [27] and the metatarsals [44,45], but it is certainly not true for the spine [66,67], the knee [28,68,69], or the ankle [40]. In particular, the lengths and moment arms of the muscles cannot be represented precisely in the model if fixed axes of rotation are assumed at each joint. The consequences of this assumption may only be minor, however. Scott and Winter [70] have shown, for example, that the relative movements of the foot and tibia can be accurately reproduced during gait when monocentric axes of rotation are assumed at the ankle and subtalar joints. Using fixed joint centers and axes of rotation to approximate the kinematic behavior of anatomical joints may therefore be reasonable for studies in human coordination.

CONCLUSIONS

The model is characterized by several key features: first, it is a model of the whole body; second, full three-dimensional motion is permitted by virtue of a 6 dof pelvis, 3 dof joints for the back and the hips, and 2 dof joints for the ankles; third, the feet are free to make and break contact with the ground; and fourth, the number of muscles is much greater than that considered in previous dynamic optimization studies. This increase in complexity has improved the fidelity of the model in a number of ways: (1) the vertical ground-reaction force demonstrates a more gradual decrease near lift-off compared with the results obtained in previous simulations [57]; (2) the fore-aft ground-reaction force is reproduced more accurately than before [57]; and (3) the model is capable of predicting not only the major movements of the body segments in the sagittal plane, but also those which occur in the frontal and transverse planes. The major limitation of the model is its failure to reproduce the kinematics of the jump near lift-off. This result may be explained by the relatively fast rise time for muscle activation used in the model. Overall, however, the high level of agreement between model and experiment validates many of the parameters assumed in the model. This work therefore lays the foundation for further studies of muscle coordination during whole-body movement. In particular, since the interaction between the feet and the ground is modeled efficiently, the model is well suited to simulating three-dimensional gait.

APPENDIX

Measurements of maximum, isometric, muscle strength were used to scale the strength of the model to the mean strength measured for the five subjects. A Biodex dynamometer was used to measure the torque at the hip, knee, and ankle as each subject performed a maximal, voluntary, isometric contraction at each joint in turn. No data were recorded for the back and abdomen muscles (see Figure A1). Prior to the experiments, the test subject warmed up on a stationary bike. The experiments were conducted on two separate days: on the first day, maximum knee-extensor and knee-flexor torques were measured; on the second day, maximum ankle-plantarflexor, ankle-dorsiflexor, hip-extensor, hip-flexor, hip-abductor, and hip-adductor torques were measured. Two contractions were given at each joint angle during

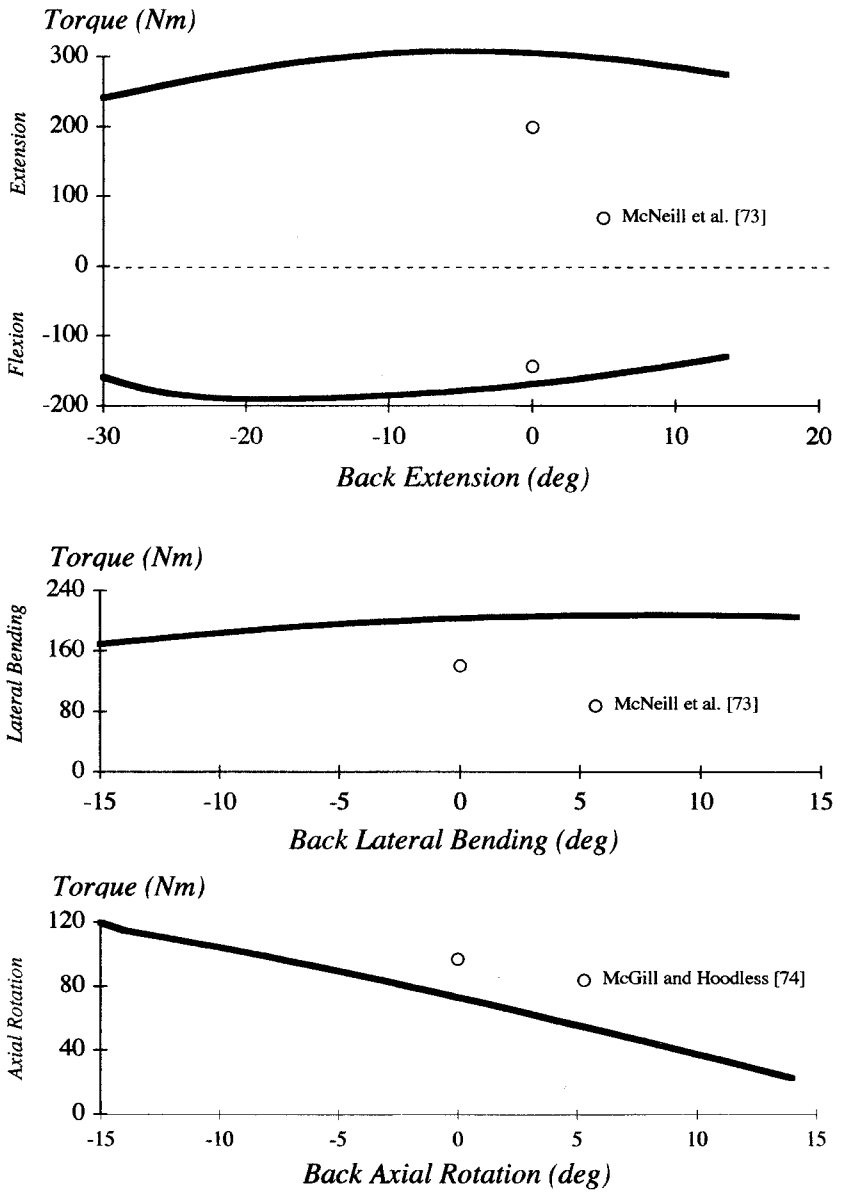

FIGURE A1 Maximum isometric torques generated at the back in the sagittal plane (flexion-extension), frontal plane (lateral bending), and transverse plane (axial rotation) for the model. Experimental data (empty circles) were obtained from the literature.

each set of experiments. The average of the two values measured at each joint angle is reported.

For the hip, maximum, voluntary, isometric extensor, flexor, abductor, and adductor torques were recorded. Hip-flexor and hip-extensor torques were measured at increments of 10°, from 90° of hip flexion to 10° of hip hyperextension (Figure A2). These data were recorded with the knee flexed to 90° and with the hip in the neutral position for both abduction-adduction and internal-external rotation. Hip-abductor and hip-adductor torques were measured with the hip abducted to 15°, with the hip adducted to 15°, and with the hip in the neutral position (Figure A2). Hip abductor-adductor torques were measured with the knee flexed to 90° and with the hip in neutral axial rotation.

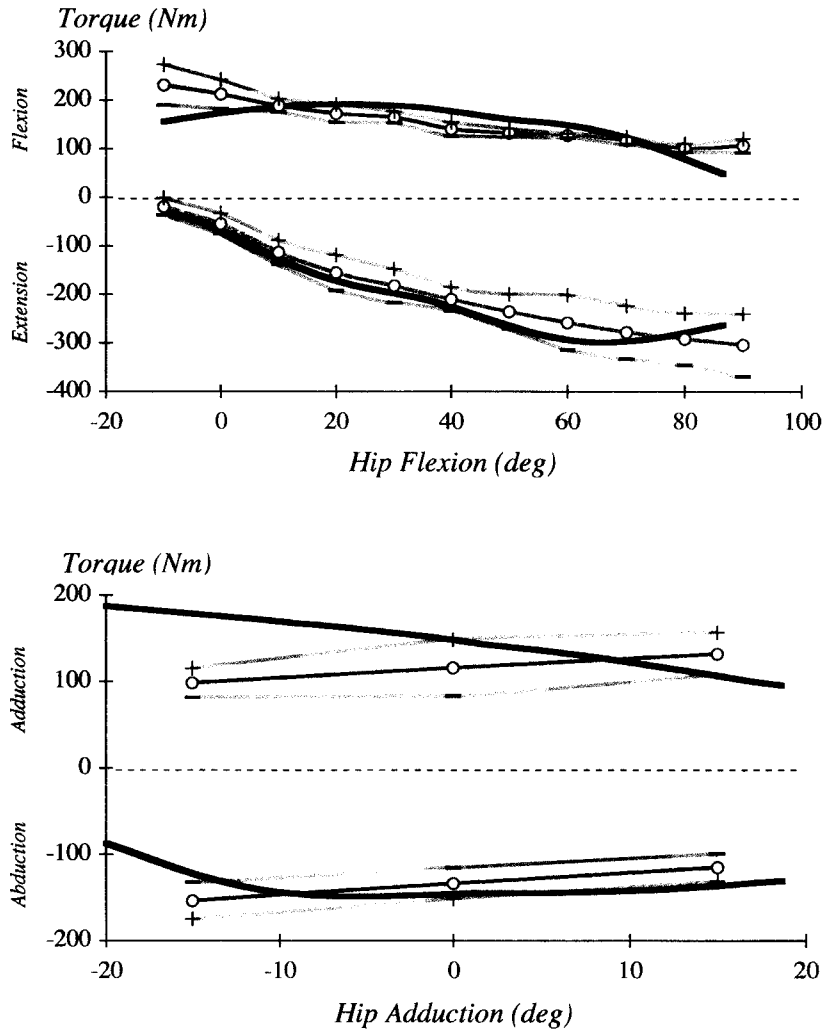

FIGURE A2 Maximum isometric torques generated at the hip in the sagittal plane (flexion-extension) and frontal plane (adduction-abduction) for the model (black lines). The grey lines define the range of maximum torques measured for the five subjects: empty circles are the mean values; + and − indicate 1 SD.

For the knee, maximum, isometric extensor torques were recorded at increments of 10°, from 90° of knee flexion to full extension (Figure A3). Maximum, isometric knee-flexor torques were also recorded from 90° of knee flexion to full extension at increments of 15°. A complete set of knee-extensor and knee-flexor torques were recorded with the hip fully extended and with the hip flexed to 60°. Only the data collected for 60° of hip flexion are presented in Figure A3; however, see Shelburne [61].

For the ankle, maximum, isometric plantarflexor and dorsiflexor torques were recorded at increments of 10°, from 40° of ankle plantarflexion to 20° of ankle dorsiflexion (Figure A3). Data were recorded with the knee fully extended and with the knee flexed to 90°. Only the data recorded for 90° of knee flexion are presented in Figure A3; however, see Shelburne [61].

The maximum isometric torques calculated for the model fall within the range of the values measured for the subjects (Figures A2 and A3). The torques generated by the back muscles (ERCSPN) were originally matched to the values reported in the literature. However, the model could not adequately extend its

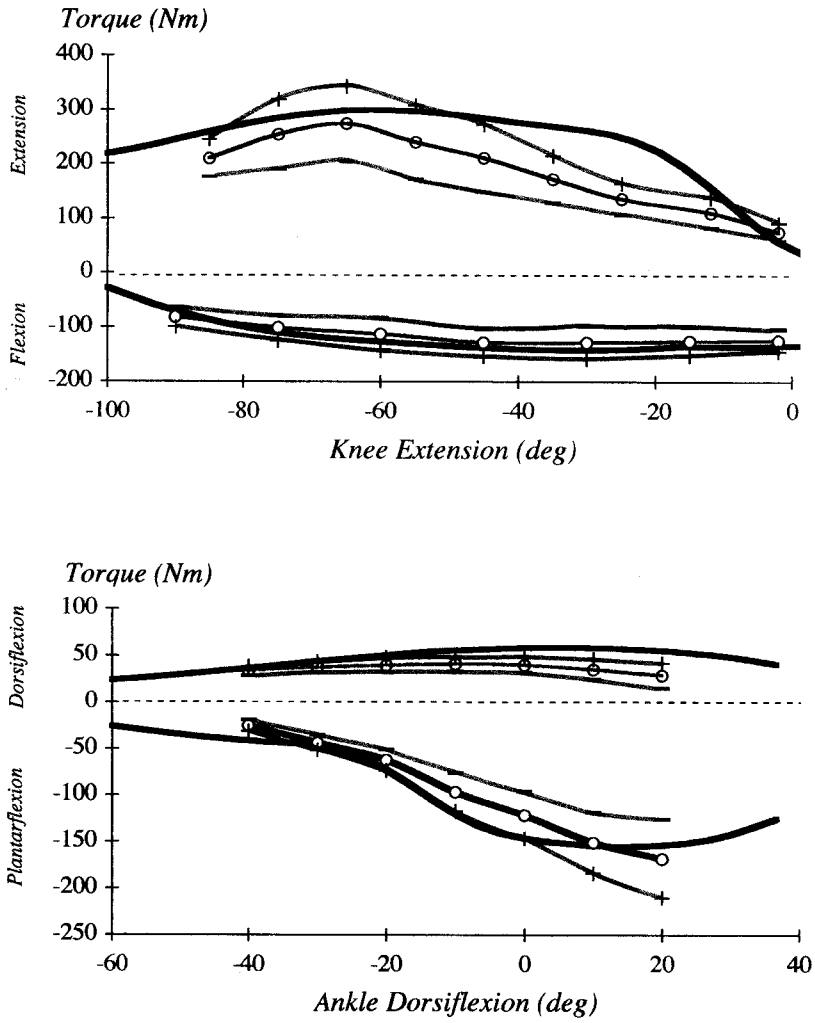

FIGURE A3 Maximum isometric torques generated at the knee (flexion-extension) and ankle (plantarflexion-dorsiflexion) in the sagittal plane for the model (black lines). The grey lines define the range of maximum torques measured for the subjects: empty circles are the mean values; + and − indicate 1 SD.

back during the jump, and so the strength of the back musculature was increased to the levels shown in Figure A1. The discrepancy between model and experiment at the back is most likely due to the fact that the kinematic behavior of the entire spine is not represented accurately in the model.

Acknowledgments

Partial funding for this work was provided by the Whitaker Foundation and by NASA, Grant # NAG5-2217. We also gratefully acknowledge the support of the National Aerospace Simulation Program at NASA/Ames Research Center and the Center for High Performance Computing at The University of Texas at Austin.

References

[1] Zajac, F. E., Wicke, R. W. and Levine, W. S. (1984). Dependence of jumping performance on muscle properties when humans use only calf muscles for propulsion. *Journal of Biomechanics*, **17**, 513–523.

[2] Davy, D. T. and Audu, M. L. (1987). A dynamic optimization technique for predicting muscle forces in the swing phase of gait. *Journal of Biomechanics*, **20**, 187–201.

[3] Khang, G and Zajac, F. E. (1989). Paraplegic standing controlled by functional neuromuscular stimulation. Part 1: Computer model and control system design. *IEEE Transactions on Biomedical Engineering*, **BME-36**, 873–884.

[4] Yamaguchi, G. T. and Zajac, F. E. (1990). Restoring unassisted natural gait to paraplegics via functional neuromuscular stimulation: A computer simulation study. *IEEE Transactions on Biomedical Engineering*, **37**, 886–902.

[5] Pandy, M. G., Zajac, F. E., Sim, E. and Levine, W. S. (1990). An optimal control model for maximum-height human jumping. *Journal of Biomechanics*, **23**, 1185–1198.

[6] Soest, A. J. van, Schwab, A. L., Bobbert, M. F. and Ingen Schenau, G. J. van (1993). The influence of the biarticularity of the gastrocnemius muscle on vertical-jumping performance. *Journal of Biomechanics*, **26**, 1–8.

[7] Zajac, F. E. (1993). Muscle coordination of movement: A perspective. *Journal of Biomechanics*, **26**(1), 109–124.

[8] Pandy, M. G., Garner, B. A. and Anderson, F. C. (1995). Optimal control of non-ballistic movements: A constraint-based performance criterion for rising from a chair. *Journal of Biomechanical Engineering*, **117**, 15–26.

[9] Anderson, F. C., Ziegler, J. M., Pandy, M. G. and Whalen, R. T. (1995). Application of high-performance computing to numerical simulation of human movement. *Journal of Biomechanical Engineering*, **117**, 155–157.

[10] Tashman, S., Zajac, F. E. and Perkash, I. (1995). Modeling and simulation of paraplegic ambulation in a reciprocating gait orthoses. *Journal of Biomechanical Engineering*, **117**, 300–308.

[11] Kautz, S. A. and Hull, M. L. (1995). Dynamic optimization analysis for equipment setup problems in endurance cycling. *Journal of Biomechanics*, **28**, 1391–1401.

[12] Anderson, F. C., Ziegler, J. M., Pandy, M. G. and Whalen, R. T. (1996). Solving large-scale optimal control problems for human movement using supercomputers. In Witten, M. and Vincent, D. J. (eds.): *Building a Man in the Machine: Computational Medicine, Public Health, and Biotechnology*. Part II. World Scientific, pp. 1088–1118.

[13] Fregly, B. J. and Zajac, F. E. (1996). A state-space analysis of mechanical energy generation, absorption, and transfer during pedaling. *Journal of Biomechanics*, **29**, 81–90.

[14] Selbie, W. S. and Caldwell, G. E. (1996). A simulation study of vertical jumping from different starting postures. *Journal of Biomechanics*, **29**, 1137–11467.

[15] Raasch, C. C., Zajac, F. E., Ma, B. and Levine, W. S. (1997). Muscle coordination of maximum-speed pedaling. *Journal of Biomechanics*, **6**, 595–602.

[16] Chow, C. K. and Jacobson, D. H. (1971). Studies of human locomotion via optimal programming. *Mathematical Biosciences*, **10**, 239–306.

[17] Hatze, H. (1976). The complete optimization of human motion. *Mathematical Biosciences*, **28**, 99–135.

[18] Seireg, A. and Arvikar, R. J. (1973). The prediction of muscular load sharing and joint forces in the lower extremities during walking. *Journal of Biomechanics*, **8**, 89–102.

[19] Crowninshield, R. D. (1978). Use of optimization techniques to predict muscle forces. *Journal of Biomechanics*, **100**, 88–92.

[20] Hardt, D. E. (1978). Determining muscle forces in the leg during human walking: An application and evaluation of optimization methods. *Journal of Biomechanical Engineering*, **100**, 72–78.

[21] Patriarco, A. B., Mann, R. W., Simon, S. R. and Mansour, J. M. (1981). An evaluation of the approaches of optimization methods in the prediction of muscle forces during human gait. *Journal of Biomechanics*, **14**, 513–525.

[22] Pennal, G. F., Conn, G. S., McDonald, G., Dale, G. and Garside, H. (1972). Motion studies of the lumbar spine. *Journal of Bone and Joint Surgery*, **54B**, 442–452.

[23] Thurston, A. J. and Harris, J. D. (1983). Normal kinematics of the lumbar spine and pelvis. *Spine*, **8**, 199–205.

[24] Pearcy, M. J. and Tibrewal, S. B. (1984). Axial rotation and lateral bending in the normal lumbar spine measured by three-dimensional radiography. *Spine*, **9**, 582–587.

[25] Stokes, V. P., Andersson, C. and Forssberg, H. (1989). Rotational and translational movement features of the pelvis and thorax during adult human locomotion. *Journal of Biomechanics*, **22**, 43–50.

[26] Anderson, F. C. (1999). A dynamic optimization solution for a complete cycle of normal gait: An analysis of muscle function and joint contact force. PhD dissertation, University of Texas at Austin, Austin, Texas.

[27] Crowninshield, R. D., Johnston, R. C., Andrews, J. G. and Brand, R. A. (1978). A biomechanical investigation of the human hip. *Journal of Biomechanics*, **11**, 75–85.

[28] Wismans, J., Veldpaus, F. and Janssen, J. (1980). A three-dimensional mathematical model of the knee-joint. *Journal of Biomechanics*, **13**, 677–685.

[29] O'Connor, J. J., Shercliff, T., Fitzpatrick, D., Bradley, J., Daniel, D., Biden, E. and Goodfellow, J. (1990). Geometry of the knee. In Daniel, D., Akeson, W. and Woo, S. (eds.): *Knee Ligament: Structure, Function, Injury, and Repair*. Raven Press, New York, pp. 163–169.

[30] Blankevoort, L., Kuiper, J., Huiskes, R. and Grootenboer, H. (1991). Articular contact in a three-dimensional model of the knee. *Journal of Biomechanics*, **24**, 1019–1031.

[31] Shelburne, K. B. and Pandy, M. G. (1997). A musculoskeletal model of the knee for evaluating ligament forces during isometric contractions. *Journal of Biomechanics*, **30**, 163–176.

[32] Pandy, M. G., Sasaki, K. and Kim, S. (1997). A three-dimensional musculoskeletal model of the human knee joint. Part 1: Theoretical construction. *Computer Methods in Biomechanics and Biomedical Engineering*, **1**, 87–108.

[33] Spoor, C. W. and van Leeuwen, J. L. (1992). Knee muscle moment arms from MRI and from tendon travel. *Journal of Biomechanics*, **25**, 201–206.

[34] Manter, J. T. (1941). Movements of the subtalar and transverse tarsal joints. *Anatomical Record*, **80**, 397.

[35] Hutter, C. G. and Scott, W. (1949). Tibial torsion. *Journal of Bone and Joint Surgery*, **31-A**, 511.

[36] Barnett, C. H. and Napier, J. R. (1952). The axis of rotation at the ankle joint in man: Its influence upon the form of the talus and the mobility of the fibula. *Journal of Anatomy*, **86**, 1–9.

[37] Isman, R. E. and Inman, V. T. (1968). Anthropometric Studies of the Human Foot and Ankle. Biomechanics Laboratory, University of California, San Francisco and Berkeley. Technical Report 58. The Laboratory, San Francisco.

[38] Inman, V. T. (1976). The Joints of the Ankle. The Williams and Wilkins Company. Baltimore.

[39] Procter, P. and Paul, J. P. (1982). Ankle joint biomechanics. *Journal of Biomechanics*, **15**, 627–634.

[40] Seigler, S., Chen, J. and Schneck, C. D. (1988). The three-dimensional kinematics and flexibility characteristics of the human ankle and subtalar joints. Part 1: Kinematics. *Journal of Biomechanical Engineering*, **110**, 364–373.

[41] Baumgarte, J. (1972). Stabilization of constraints and integrals of motion. *Computer and Mathematical Applications in Mechanical Engineering*, **1**, 1–16.

[42] Hatze, H. (1981). A comprehensive model for human motion simulation and its application to the take-off phase of the long jump. *Journal of Biomechanics*, **14**, 135–142.
[43] Meglan, D. A. (1991). Enhanced analysis of human locomotion. PhD dissertation, Ohio State University, Columbus, Ohio.
[44] Scott, S. H. and Winter, D. A. (1993). Biomechanical model of the human foot: Kinematics and kinetics during the stance phase of walking. *Journal of Biomechanics*, **26**, 1091–1104.
[45] Gilchrist, L. A. and Winter, D. A. (1996). A two-part, viscoelastic foot model for use in gait simulations. *Journal of Biomechanics*, **29**, 795–798.
[46] McConville, J. T., Clauser, C. E., Churchill, T. D., Cuzzi, J. and Kaleps, I. (1980). Anthropometric relationships of body and body segment moments of inertia. Technical Report AFAMRL-TR-80-119. Air Force Aerospace Medical Research Laboratory, Wright-Patterson AFB, Ohio.
[47] Delp, S. L. (1990). Surgery simulation: A computer graphics system to analyze and design musculoskeletal reconstructions of the lower limb. Ph.D. disseration, Stanford University, Stanford, California.
[48] Winter, D. A. (1979). Biomechanics of Human Motion. John Wiley, New York.
[49] Audu, M. L. (1985). Optimal control modeling of lower extremity musculoskeletal motion. Ph.D. Dissertation. Case Western University, Cleveland, Ohio.
[50] Zajac, F. E. (1989). Muscle and tendon: Properties, models, scaling, and application to biomechanics and motor control. In Bourne, J. R. (ed.): *CRC Critical Reviews in Biomedical Engineering*, **19**, pp. 359–411, CRC Press, Boca Raton.
[51] Pandy, M. G., Anderson, F. C. and Hull, D. G. (1992). A parameter optimization approach for the optimal control of large-scale musculoskeletal systems. *Journal of Biomechanical Engineering*, **114**, 450–460.
[52] Reicher, M. A. (1993). An atlas of normal multiplanar anatomy of the knee joint. In Mink, J. H., Reicher, M. A., Crues, J. V. and Deutsch, A. L. (eds): *MRI of the Knee*. Raven Press, New York, pp. 51–90.
[53] Symbolic Dynamics (1992). SD/Fast User's Manual, Version B.1.1.
[54] Bryson, A. E. and Ho, Y. C. (1975). Applied Optimal Control: Optimization, estimation, and control. Hemisphere Publishing Corp., New York.
[55] Powell, M. J. (1978). A fast algorithm for nonlinearly constrained optimization calculations. In Matson, G. A. (ed.): *Numerical analysis: Lecture notes in mathematics*, **630**, 144–157, Springer-Verlag.
[56] Craig, J. J. (1986). Introduction to Robotics: Mechanics and Control. Addison-Wesley Publishing, Massachusetts.
[57] Pandy, M. G. and Zajac, F. E. (1991). Optimal muscular coordination strategies for jumping. *Journal of Biomechanics*, **24**, 1–10.
[58] Desmedt, J. E. and Godaux, E. (1977). Ballistic contractions in man: characteristic recruitment pattern of single motor units of the tibialis anterior muscle. *Journal of Physiology*, **264**, 673–693.
[59] Anderson, F. C. and Pandy, M. G. (1993). Storage and utilization of elastic strain energy during jumping. *Journal of Biomechanics*, **26**, 1413–1427.
[60] Ziegler, J. M. and Pandy, M. G. (1995). A computational model for determining muscle-ligament interactions at the knee during movement. In Witten, M. (ed.): *Building a Man in the Machine: Computational Medicine, Public Health, and Biotechnology*. Part I. World Scientific, New Jersey, pp. 532–568.
[61] Shelburne (1996). Modeling the mechanics of the normal and reconstructed knee joint. PhD dissertation, University of Texas at Austin, Austin, Texas.
[62] Gray, H. (1977). Gray's anatomy. Edited by Pickering, T., Howden, R, Gramercy Books, New Jersey.
[63] Duda, G. N., Schneider, E. and Chao, E. Y. (1997). Internal forces and moments in the femur during walking. *Journal of Biomechanics*, **30**, 933–941.
[64] Pedersen, D. R., Brand, R. A. and Davy, D. T. (1997). Pelvic muscle and acetabular contact forces during gait. *Journal of Biomechanics*, **30**, 959–965.
[65] Gregersen, G. G. and Lucas, D. B. (1967). An in-vivo study of the axial rotation of the human throacolumbar spine. *Journal of Bone and Joint Surgery*, **49A**, 247–262.
[66] Pearcy, M. J. and Bogduk, N. (1988). Instantaneous axes of rotation of the lumbar intervertebral joints. *Spine*, **13**, 1033–1041.
[67] Panjabi, M. M., Krag, M. H., Dimnet, J. C., Walter, S. D. and Brand, R. A. (1984). Thoracic spine centers of rotation in the sagittal plane. *Journal of Orthopaedic Research*, **1**, 387–394.
[68] Walker, P. S., Shoji, H. and Erkman, M. J. (1972). The rotational axis of the knee and its significance to prosthesis design. *Clinical Orthopaedics and Related Research*, **89**, 160–170.
[69] Blankevoort, L., Huiskes, R. and DeLange, A. (1990). Helical axes of passive knee joint motions. *Journal of Biomechanics*, **23**, 1219–1229.
[70] Scott, S. H. and Winter, D. A. (1991). Talocrural and talocalcaneal joint kinematics and kinetics during the stance phase of walking. *Journal of Biomechanics*, **24**, 743–752.
[71] Levine, W. S., Zajac, F. E., Belzer, M. R. and Zomlefer, M. R. (1983). Ankle controls that produce a maximal vertical jump when other joints are locked. *IEEE Transactions on Automatic Control*, **AC-28**, 1008–1016.
[72] Marshall, R. N., Wood, G. A. and Jennings, L. S. (1989). Performance objectives in human movement: A review and application to the stance phase of normal walking. *Human Movement Science*, **8**, 571–594.
[73] McNeill, T., Warwick, D., Andersson, G. and Schultz, A. (1980). Trunk strengths in attempted flexion, extension, and lateral bending in healthy subjects and patients with low-back disorders. *Spine*, **5**, 529–538.
[74] McGill, S. M. and Hoodless, K. (1980). Measured and modeled static and dynamic axial trunk torsion during twisting in males and females. *Journal of Biomedical Engineering*, **12**, 403–409.